# A model for eastward and westward jets in laboratory experiments and planetary atmospheres

P. S. Marcus and C. Lee[a)]
*University of California, Berkeley, California 94720*

(Received 12 September 1995; accepted 21 October 1997)

Flows in a rotating annular tank [J. Sommeria, S. D. Meyers, and H. L. Swinney, *Nonlinear Topics in Ocean Physics*, edited by A. Osborne (North Holland, Amsterdam, 1991); Nature (London) **337**, 58 (1989); T. H. Solomon, W. J. Holloway, and H. L. Swinney, Phys. Fluids A **5**, 1971 (1993); J. Sommeria, S. D. Meyers, and H. L. Swinney, Nature (London) **331**, 689 (1989)] with a sloping bottom (that simulates a barotropic atmosphere's Coriolis force with a topographic $\beta$-effect [J. Pedlosky, *Geophysical Fluid Dynamics*, 2nd ed. (Springer, Berlin, 1986)]) produce eastward and westward jets, i.e., azimuthal flows moving in the same or opposite direction as the annulus' rotation. Flows are forced by pumping fluid in and out of two concentric slits in the bottom boundary, and the direction of the jets depends on the direction of the pumping. The eastward and westward jets differ, with the former narrow, strong, and wavy. The jets of Jupiter and Saturn have the same east–west asymmetry [P. S. Marcus, Ann. Rev. Astron. Astro. **431**, 523 (1993)]. Numerical simulations show that the azimuthally-averaged flow differs substantially from the non-averaged flow which has sharp gradients in the potential vorticity $q$. They also show that the maxima of the eastward jets and Rossby waves are located where the gradients of $q$ are large, and the maxima of the westward jets and vortex chains are located where they are weak. As the forcing is increased the drift velocities of the two chains of vortices of the eastward jet lock together; whereas the two chains of the westward jet do not. Inspired by a previously published, [P. S. Marcus, Ann. Rev. Astron. Astro. **431**, 523 (1993)] piece-wise constant-$q$ model of the Jovian jets and based on numerical simulations, a new model of the experimental flow that is characterized by regions of undisturbed flow and bands of nearly uniform $q$ separated by sharp gradients is presented. It explains the asymmetry of the laboratory jets and quantitatively describes all of the wave and vortex behavior in the experiments including the locking of the vortex chains of the eastward jet. The simulations and new model contradict the predictions of a competing, older model of the laboratory flow that is based on a Bickley jet; this raises concerns about previous calculations of Lagrangian mixing in the laboratory experiments that used the Bickley model for the fluid velocity. The new model, simulations and laboratory experiments all show that jets can be formed by the mixing and homogenization of $q$. The relevance of this to the jets of Jupiter is discussed. © *1998 American Institute of Physics.* [S1070-6631(98)01405-6]

## I. INTRODUCTION

In laboratory flows in rotating annuli that were designed to simulate an atmosphere, eastward jets of fluid differed strikingly from westward jets.[1–4] Here, eastward (westward) is defined as moving in the same (opposite) direction as the annulus' rotation.[7] The bottom boundary of the annulus was radially sloping with two concentric slits. The flow was forced by pumping fluid in one slit and withdrawing it from the other. A jet formed between the slits and its direction depended on the direction of the pumping. As the forcing increased, the jet's two sides became wavy and each side spawned a chain of vortices. From a geophysical perspective the most significant asymmetry between the jets was that eastward jets were narrower, stronger, and more wavy; the same asymmetry occurs in planetary atmospheres, c.f., the nearly axisymmetric Jovian east–west winds where their direction alternates with latitude[6,8,9] (fig. 1), and Saturn's winds[10] including its north polar jet.[11] A similar asymmetry in the earth's atmosphere[5] is that strong jets are always eastward and wavy, c.f., the winter, polar, stratospheric jets and the mid-latitude, upper tropospheric jet streams. (The earth's westward, return circulations are so broad and weak that they are not identified as jets.) Although east–west atmospheric asymmetries have been numerically simulated,[6,8] their explanation remains controversial. In the laboratory the most obvious asymmetry of the jets is the dynamics of their vortex chains. As the flow's forcing is increased, the drift speeds of the two chains of the eastward jet lock together; whereas the speeds of the two chains of the westward jet, though closer to each other than those of the eastward jet, remain different.

Our primary goal is to explain the laboratory experiment and our secondary goal is to determine what relevance, if any, its physics has to the geophysical flows that originally motivated the experiments. To do this, we first numerically

[a)]Present address: Dept. of Mechanical Engineering, University of Seoul, 90 Jeonnong-dong, Dongdaemun-gu, Seoul, 130-743, Korea.

 © 1998 American Institute of Physics

Downloaded 12 Jul 2011 to 169.229.32.136. Redistribution subject to AIP license or copyright; see http://pof.aip.org/about/rights_and_permissions

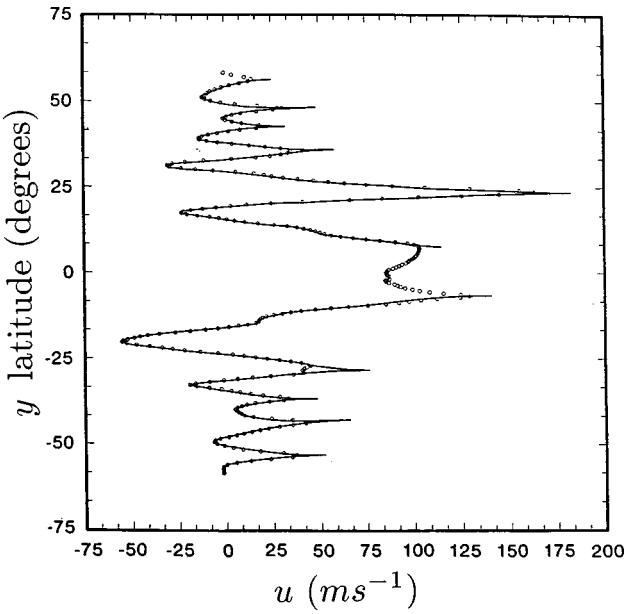


FIG. 1. Jovian east–west velocity $u$ as a function of latitude $y$. The circles are the measurements[9] and the solid curve is a theoretical fit.[6] The velocity is not QG near the equator, so there is no QG fit.

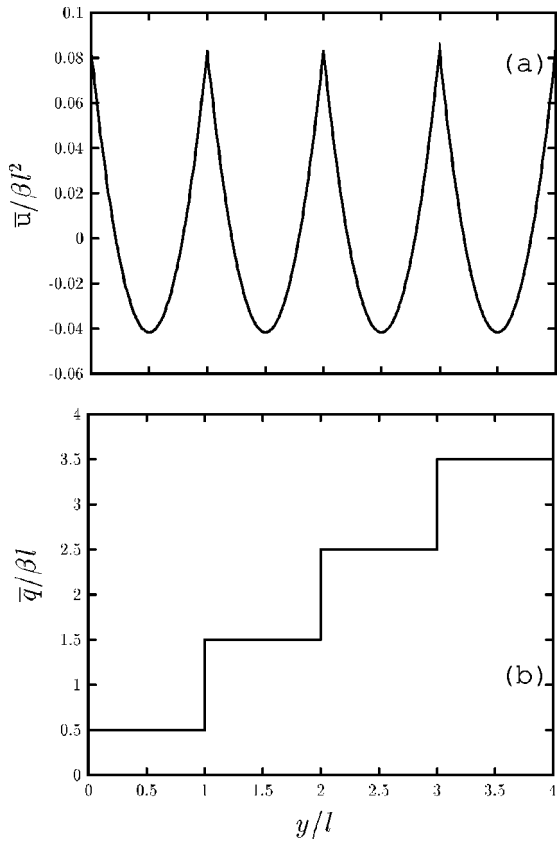


FIG. 2. (a) Model $u(y)$ as a function of latitude $y$ for the jovian east–west velocity inferred from vortex dynamics.[6] Eastward (westward) jets have $u>0$ ($u<0$). The $u$ is piecewise parabolic. (b) the $q(y)\equiv\beta y-du/dy$ for (a). This $u$ and $q$ also model the flow in an experiment with multiple slits in the bottom boundary (see section VII). Near each slit a region with uniform $q$ grows in size until it runs into its neighbor. This creates a step function in $q$ with step width $l$ and step height $\Delta\overline{q}=\beta l$. As in the model in figs. 8 and 9, $q=\beta y$ when there is no pumping. In the model, eastward jets are always located at the maxima of $|\nabla q|$ and the westward jets at the minima.

simulate the flows to obtain information not readily available from experiments, c.f. instantaneous flow velocities **U** and potential vorticities $q$. (One point of this paper is that averaged values of **U** and $q$ are misleading.) With this insight we construct a model that quantitatively reproduces the experiments. Most of this paper is devoted to validating our model and comparing it to a competing model based on a Bickley jet.[2,3,12] Determining which model is correct is important for several reasons. These laboratory flows have been used as examples of the Hamiltonian dynamics of passive Lagrangian tracers.[12] When seeded with tracers, the flows show regions of complete mixing as well as barriers through which the mixing cannot penetrate. Current theoretical analyses of the mixing in the experiment are based on model flows rather than the laboratory or numerically simulated velocities. The experiments, simulations, and our model all have sharp gradients in $q$, which are known to act as barriers to mixing; whereas the competing models, including the Bickley jet, have smooth $q$. For this reason and because the Bickley jet and other models fail to capture the vortex dynamics in the experiments, questions arise about the validity of the mixing analyses.

Our second goal is to relate the experiments and our model to planetary atmospheres. Although there are many important differences between these laboratory experiments and atmospheres, not the least of which is the forcing, there are fundamental issues such as vortex dynamics and mixing which the experiments address. The key idea of our model is that mixing ''homogenizes'' the $q$ into azimuthal bands with piece-wise constant $q$ that are separated by sharp gradients.[13] As the forcing increases, the bands grow and merge and the model flow changes. Little work has been done previously on how (or if) $q$ is homogenized or how east–west jets are created and maintained in forced/dissipated systems (i.e., not run-down experiments that have no forcing). The laboratory experiments simulated here address both issues. Curiously, the first step in constructing our model for the laboratory flow came from jovian observations. (Because it is impossible to measure $q$ directly in the jovian atmosphere—and difficult in laboratory flows—we used *indirect* methods based on the properties of the planetary vortices to find the $q$ of the jets—see section VII.) We developed a piece-wise constant-$q$ model for the jovian jets, which in terms of the more general model presented here corresponds to the case with large forcing (fig. 2). The model was inferred only from observations rather than from any consideration of dynamics or homogenization of $q$. It was our curiosity of how and why the empirically-derived model might form that led to our interest in these laboratory experiments and that provided the impetus for the dynamic model presented here. Thus, one goal of this paper is to show that the laboratory experiments and the simulations prove that east–west jets can be created by the homogenization of $q$ and thereby show that our jet model for Jupiter is plausible.

The outline of the paper is as follows. In section II we summarize the laboratory experiments. In section III we present the quasi-geostrophic (QG) equations that govern both the laboratory experiment and planetary atmospheres.

Downloaded 12 Jul 2011 to 169.229.32.136. Redistribution subject to AIP license or copyright; see http://pof.aip.org/about/rights_and_permissions

Piecewise analytic approximations to and numerical solutions of the primary flows are presented. Section IV contains our model of the east–west winds and its measurable consequences (wave speeds, vortex locations, etc.). In section V we compare our model with numerical solutions of the QG equations and with the laboratory experiments. A comparison with the Bickley jet model is given in section VI and our conclusions along with their relevance to planetary atmospheres is in section VII. Validation of our physical approximations appear in the Appendix.

## II. SUMMARY OF LABORATORY EXPERIMENTS AND NUMERICAL SIMULATIONS

The laboratory experiment[3] used a constant-density fluid in a wide-gap annulus where the top, bottom, and sides all rotated at the same fast angular velocity $f/2$. Flows were forced by pumping fluid through axisymmetric, concentric slits (see the Appendix) of thickness $L^{slit}$ at radii $R_1^{slit}$ and $R_2^{slit}$ in the bottom boundary where $R_1^{slit}<R_2^{slit}$. The bottom of the annulus had slope $s$ so that the depth at the outer radius $R_{out}$ was greater than at the inner radius $R_{in}$. This produced a topographic $\beta$-effect[5] to model the gradient of the atmosphere's Coriolis force. The laboratory experiment was designed to be an analog of a one-layer, constant density atmosphere in which the pumping through the bottom boundary simulated the convective overshoot of plumes from an underlying unstable layer.

The laboratory experiments and our subsequent numerical calculations[14] (carried out with the same geometry and other flow parameters[15]) are in good agreement and summarized as follows: For low pumping rates $P$, a vortex layer forms above each slit which in turn creates the primary flow: an axisymmetric, azimuthal jet at $R_1^{slit}\leqslant r\leqslant R_2^{slit}$. When fluid is pumped *into* the tank at $R_2^{slit}$ and removed at $R_1^{slit}$, the jet travels in the same direction as the rotating tank and is defined to be *eastward*. When the direction of the pumping is reversed, the jet is *westward*. For $P\geqslant P_{crit}$, the approximate discontinuity in the velocity $\mathbf{U}$ at the inner edge of the jet creates unstable, non-axisymmetric (Kelvin–Helmholtz-like and Rossby wave) eigenmodes, and the vortex layer at $R_1^{slit}$ becomes wavy. As $P$ is increased, nonlinearities roll up the vortex layer creating a vortex chain at $R_1^{slit}$ (fig. 3a). For slightly greater $P$, instabilities of the outer layer create a second vortex chain at $R_2^{slit}$ (fig. 3b). Our numerical calculations show that the two chains travel azimuthally around the annulus with different speeds $c_1$ and $c_2$, and the flows are temporally quasi-periodic with form

$$\mathbf{U}=\sum_{j=-\infty}^{\infty}\sum_{n=-\infty}^{\infty}\mathbf{a}_{j,n}(r)\exp\{[ijm_1(\phi-c_1t)]+[inm_2(\phi-c_2t)]\}. \tag{1}$$

The subscript $i$ refers to quantities associated with $R_i^{slit}$, where $i=1,2$.

The westward jet has a smaller $P_{crit}$ than the eastward jet, and the nonlinear evolutions of the two jets differ greatly. As $P$ is increased, the westward jet's two vortex chains move closer together in radius, while the eastward jet's chains move apart. At $P/P_{crit}\simeq 1.5$ the westward jet's two vortex chains overlap radially. The $c_i$ of the chains of the eastward jets are positive while those of the westward are negative. (Values of $c_i$ are in the annular tank's rotating frame. Without loss of generality, the tank's angular velocity is positive.) For the eastward jet, as $P$ is increased above $P_{lock}$ the two vortex chains lock together, so $c_1=c_2$, and the numerical calculations show that the flow is temporally periodic (or steady to a viewer rotating with speed $c_1$). See fig. 4. The locking of the eastward jets is easy to identify in the laboratory because it is accompanied by an abrupt decrease in $c_i$ of $\sim 50\%$. Our numerical calculations show the locking is robust; it occurs over a wide range in $P$ and other parameters (such as the widths of the slits in the bottom). The laboratory experiments were unable to determine whether the westward jets' two vortex chains locked. Our numerical calculations show that the westward chains lock only for a

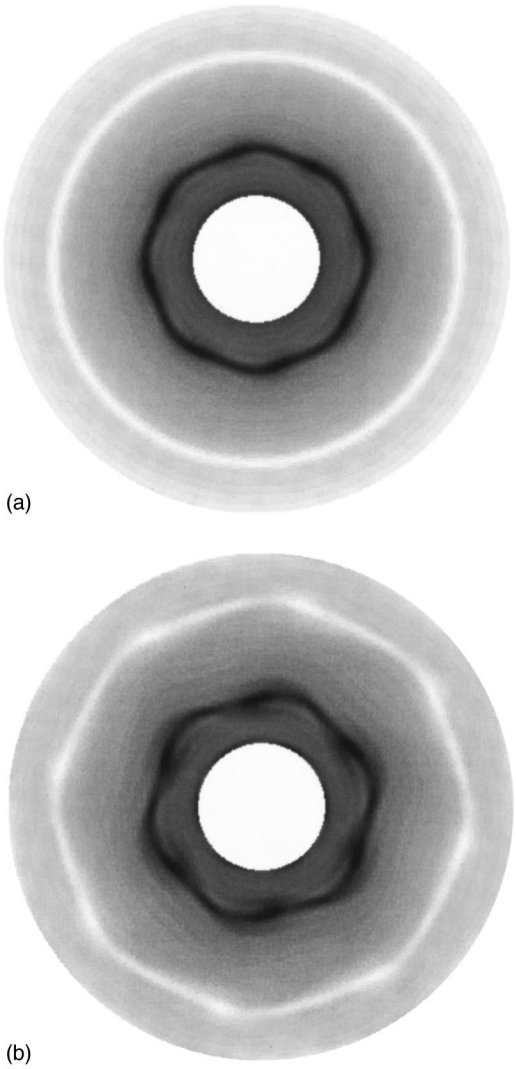


FIG. 3. Numerically computed potential vorticity $q$ (using a grey scale with $q>0$ dark and $q<0$ light) of the unlocked eastward (counter-clockwise) flows with (a) $P=50$ and (b) $P=80$ cm$^3$ s$^{-1}$. The jet is between $R_1^{slit}$ and $R_2^{slit}$ which are coincident with the light and dark rings of $q$. The vortices at $R_1^{slit}$ have $\omega>0$ and those at $R_2^{slit}$ have $\omega<0$. The parameters[15] are $R_1^{slit}=18.9$, $\nu=0.1$, $f=4\pi$ (All units CGS).

Downloaded 12 Jul 2011 to 169.229.32.136. Redistribution subject to AIP license or copyright; see http://pof.aip.org/about/rights_and_permissions

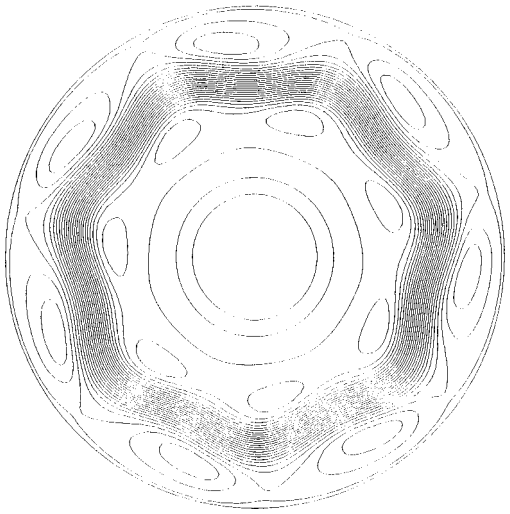

FIG. 4. Stream function $\psi$ of the numerically computed[15] locked eastward jet with $P=44$ viewed in the rotating frame where the flow is steady. See Table II. $R_1^{slit}=27.0$, $\nu=0.033$, and $f=6\pi$. Because the flow is steady the contours of constant $q$ and $\psi$ are nearly the same. There is only one approximate discontinuity in $q$, and the Rossby wave located there makes it wavy. The two vortex chains are in regions where $\nabla q \neq 0$ and are separated from each other by the approximate discontinuity of $q$. The signs of the vortices are the same as that of the local shear of the jet. Thus, all of the vortices in the inner chain have $\omega>0$, while those in the outer have $\omega<0$.

small range of $P$ and only when the widths of the slits in the bottom are carefully tuned. When westward jets' chains lock in the numerical calculations, the $c_i$ do not change and the numbers of vortices in the two chains are very different. See fig. 5. In contrast, the numbers of vortices in the locked eastward jets' two chains are nearly the same, and they never overlap radially. See fig. 4. Thus, the locking of chains is qualitatively different for eastward and westward jets. For $P>2P_{crit}$, the eastward and westward jets differ greatly. The numerical calculations show that the time-averaged potential vorticity $q$ of the westward jet is nearly uniform, and the jet nearly fills the annulus. Embedded within it are a few large, robust vortices with vorticity of the same sign as the shear of the ambient jet. As $P$ is increased further, the vortices merge leaving a single vortex. (The laboratory experiment[4] of the westward jet and vortex at large $P$ were a test of theoretical and numerical predictions of Jupiter's Great Red Spot.[16]) In contrast, the eastward flow at large $P$ evolves into a strong, narrow, wavy jet with a radial location approximately midway between the two slits. The large amplitude Rossby wave on the jet causes its radial location to meander in azimuthal angle $\phi$. This flow has been used to model the Antarctic stratospheric polar vortex.[1]

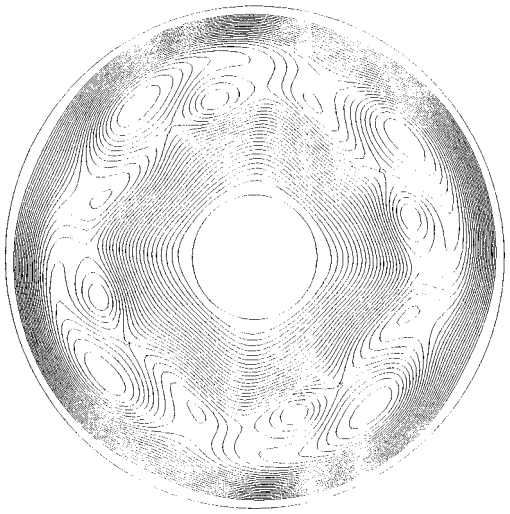

FIG. 5. Same control parameters as in fig. 4 but for the locked westward jet. See Table III. There are 8 small, negative vortices in the inner chain and 4 large, positive vortices in the outer chain. Thus, the signs of the vortices are the same as that of the local shear of the jet. Because $P>P_{west}^{link}=21.4$, the two regions of uniform $q$ are joined together and the numerically computed flow looks like the model flow in fig. 9f. Because the flow is steady in this frame, the contours of constant $q$ and $\psi$ are nearly the same, and the strong gradients in $\psi$ coincide with the two approximate discontinuities in $q$. The two weak Rossby waves are centered near the maxima of $|\nabla q|$; while the vortices are near the minimum of $|\nabla q|$.

Although there is a strong asymmetry between the eastward and westward jets, it should be noted that in the QG limit (see section III), *axisymmetric* eastward and westward flows with the same $P$ are mirror images, and their velocities $|\mathbf{U}|$ are independent of $s$. So there is no east–west asymmetry for axisymmetric flows (though their non-axisymmetric eigenmodes and eigenvalues are east–west asymmetric). With $s=0$—even when the flows are non-axisymmetric and non-linear—the eastward and westward jets and their vortex chains are mirror images of each other. It is the non-zero $s$ (or $\beta$ in the atmosphere) coupled with the loss of axisymmetry that breaks the east–west symmetry.

## III. EQUATIONS AND THE PRIMARY FLOW

Rather than solve the three-dimensional Navier–Stokes equation with boundary conditions for the inflow and outflow slits in the bottom of the annular tank, we use the first integral of the two-dimensional, quasi-geostrophic (QG) equation along with an Ekman boundary layer (or equivalently with Rayleigh friction):

$$D\mathbf{U}/Dt = -\nabla\Pi/\rho + \beta r\mathbf{U}\times\hat{\mathbf{z}} + \nu\nabla^2\mathbf{U} - \mathbf{U}/\tau + \mathbf{F}, \qquad (2)$$

where $\mathbf{U}(r,\phi,t)$ is the velocity, $D/Dt \equiv (\partial/\partial t + \mathbf{U}\cdot\nabla)$ is the advective derivative, $\rho$ is the constant density of the fluid, $\Pi$ is the pressure head that forces $\nabla\cdot\mathbf{U}\equiv 0$, $\hat{\mathbf{z}}$ is a unit vector, $\nu$ is the kinematic viscosity, $\beta \equiv sf/H$, $H$ is the mean depth of the tank, $f$ is the Coriolis parameter equal to twice the angular velocity of the tank, and $\tau \equiv H/\sqrt{2\nu|f|}$ is the Ekman spin-down time (or Rayleigh damping time). The flow is 2-dimensional, such that $\hat{\mathbf{z}}\cdot\mathbf{U}\equiv 0$ and $\partial\mathbf{U}/\partial z \equiv 0$. The forcing $\mathbf{F}$ of the quasi-geostrophic component of the flow due to pumping the fluid through the slits in the bottom boundary and creating a weak ageostrophic flow is[17]

$$\mathbf{F}(r) = -\left[\frac{f}{rH}\int_{R_{in}}^{r} \mathrm{w}(r')r'dr'\right]\hat{\boldsymbol{\phi}}, \qquad (3)$$

where $\mathrm{w}(r)$ is the vertical velocity of the fluid entering through the slit and $\hat{\boldsymbol{\phi}}$ is a unit vector. Conservation of mass requires $\int_{R_{in}}^{R_{out}}\mathrm{w}(r')r'dr' = 0$. The value of $\mathrm{w}(r)$ is zero ex-

Downloaded 12 Jul 2011 to 169.229.32.136. Redistribution subject to AIP license or copyright; see http://pof.aip.org/about/rights_and_permissions

cept at the slits, and the total pumping rate $P$ is defined as $P \equiv \pi \int_{R_{in}}^{R_{out}} |\mathrm{w}(r')| r' dr'$. The boundary condition for Eq. (2) is that $\mathbf{U}=0$ at $R_{in}$ and $R_{out}$. The curl of (2) gives the equation for the potential vorticity $q \equiv (\omega + \beta r)$ where $\omega \equiv \hat{\mathbf{z}} \cdot \nabla \times \mathbf{U}$:

$$Dq/Dt = -\omega/\tau + \nu \nabla^2 \omega - f\mathrm{w}(r)/H. \tag{4}$$

For these QG equations to be valid, the Rossby number $\epsilon \equiv V/fL \ll 1$, $1/(fT) \leq \epsilon$, $\beta L/f \leq \epsilon$, and $\mathrm{w}/Hf \leq \epsilon^2$, where $V$, $T$, and $L$ are the characteristic velocity, time and length of the flow.[5] The QG approximation is supported by the laboratory experiments which show that $\partial \mathbf{U}/\partial z \simeq 0$. When $s=0$ equation (2) has a symmetry: The flow is invariant under $\mathrm{w} \to -\mathrm{w}$, $u(r,\phi) \to -u(r,-\phi,t)$ and $v(r,\phi) \to v(r,-\phi)$ (where $u \equiv \hat{\phi} \cdot \mathbf{U}$ and $v \equiv \hat{\mathbf{r}} \cdot \mathbf{U}$), so eastward and westward jets are mirror images of each other. A finite $s$ (or $\beta$) breaks the symmetry.

There is a steady, axisymmetric, primary flow for all $P$ with $v=0$ and

$$u(r) = -\frac{f\tau}{rH} \int_{R_{in}}^{r} r' \mathrm{w}(r') dr' + \tau \nu (\nabla^2 - 1/r^2) u \tag{5}$$

and

$$\omega(r) = -f\tau \mathrm{w}(r)/H + \tau \nu \nabla^2 \omega. \tag{6}$$

In the limit of approximating the slits as delta functions, we obtain

$$\mathrm{w}(r) = \pm \frac{P}{2\pi} [\delta(r - R_1^{slit})/R_1^{slit} - \delta(r - R_2^{slit})/R_2^{slit}]. \tag{7}$$

Assuming the dissipation due to $\nu$ (but not due to $\tau$) is negligible and using equation (7) gives the model for the primary flow:

$$\overline{\omega}(r) = \mp \frac{f\tau P}{2\pi H} [\delta(r - R_1^{slit})/R_1^{slit} - \delta(r - R_2^{slit})/R_2^{slit}] \tag{8}$$

$$\overline{u}(r) = \begin{cases} 0 & \text{for } r < R_1^{slit}, \\ \mp \dfrac{fP\tau}{2\pi r H} & \text{for } R_1^{slit} \leq r \leq R_2^{slit}, \\ 0 & \text{for } r > R_2^{slit}. \end{cases} \tag{9}$$

*An overbar denotes the model, rather than exact or numerical solution.* The upper signs in equations (7)–(9) are for $\mathrm{w}(R_1^{slit}) > 0$, *ie,* for westward jets. The primary $r\overline{u}(r)$ is a top-hat. Figure 6 shows a comparison between $\overline{u}(r)$ and the numerical solution of equation (5).

For simplicity, we use a Cartesian rather than annular geometry in modeling the flows in the laboratory annulus and in the numerical calculations. In Cartesian geometry, $r$ in equation (2) is replaced with $(-y)$ and $r\phi$ with $x$. We also replace $R_i^{slit}$ with $Y_i^{slit}$, $R_{in}$ with $Y_{in}$, and $R_{out}$ with $Y_{out}$. With Cartesian coordinates, $u \equiv \hat{\mathbf{x}} \cdot \mathbf{U}$ and $v \equiv \hat{\mathbf{y}} \cdot \mathbf{U}$. Subscripts ''1'' and ''2'' are switched so that $Y_{in} < Y_1^{slit} < Y_2^{slit} < Y_{out}$. In Cartesian geometry equation (3) is replaced with

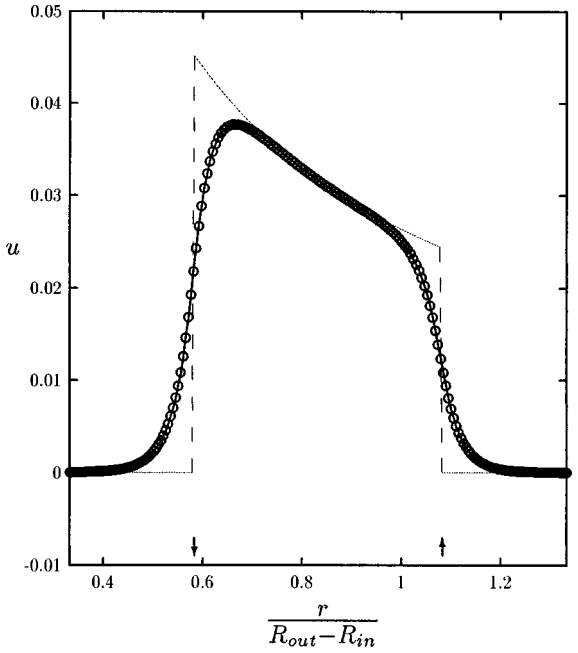


FIG. 6. The unstable, axisymmetric, primary flow $u(r)$ computed from equation (5) with 257 radial Chebyshev collocation points (open circles) compared with the model $\overline{u}$ (broken curve) in equation (9) at $P=47.7$, $\nu=0.1$, $f=4\pi$ and $R_1^{slit}=18.9$. At these parameter values,[15] $P_{crit}=44.0$ for the eastward flow. The vertical arrows near the $r$-axis represent the locations and directions of the pumping through the bottom slits. The finite thickness of the bottom slit acts with $\nu$ to broaden the sides of the top-hat function by the slit thickness plus a fraction[18] of the Stewartson layer thickness $\sqrt{\tau\nu}$. Here the velocity is plotted in units of $\beta(R_{out}-R_{in})^2$.

$$\mathbf{F}(y) = \frac{f}{H} \int_{Y_{in}}^{y} \mathrm{w}(y') dy' \hat{\mathbf{x}}. \tag{10}$$

In Cartesian geometry the model primary flow in equation (9) becomes

$$\overline{u}(y) = \begin{cases} 0 & \text{for } y < Y_1^{slit}, \\ \pm V_0 & \text{for } Y_1^{slit} \leq y \leq Y_2^{slit}, \\ 0 & \text{for } y > Y_2^{slit} \end{cases} \tag{11}$$

with

$$\overline{\omega}(y) = \pm V_0 [\delta(y - Y_2^{slit}) - \delta(y - Y_1^{slit})], \tag{12}$$

where

$$V_0 \equiv f\tau \mathscr{P}/H, \tag{13}$$

$\mathscr{P}$ is the absolute value of the volume of fluid per unit time per unit length in $x$ pumped through a slit and $q \equiv \omega + \beta y$. The upper sign in equations (11) and (12) is for eastward jets. For the Cartesian model, the coordinate origin is chosen to be midway between the two slits, so $Y_1^{slit} \equiv -Y_2^{slit}$. Thus, the primary flow $\overline{u}(y)$ is symmetric in $y$ while $\overline{\omega}(y)$ and $\overline{q}(y)$ are anti-symmetric. Equations (5) and (11) show that the primary flow is independent of $\beta$ and that $|u|$ is the same for eastward and westward jets.

Downloaded 12 Jul 2011 to 169.229.32.136. Redistribution subject to AIP license or copyright; see http://pof.aip.org/about/rights_and_permissions

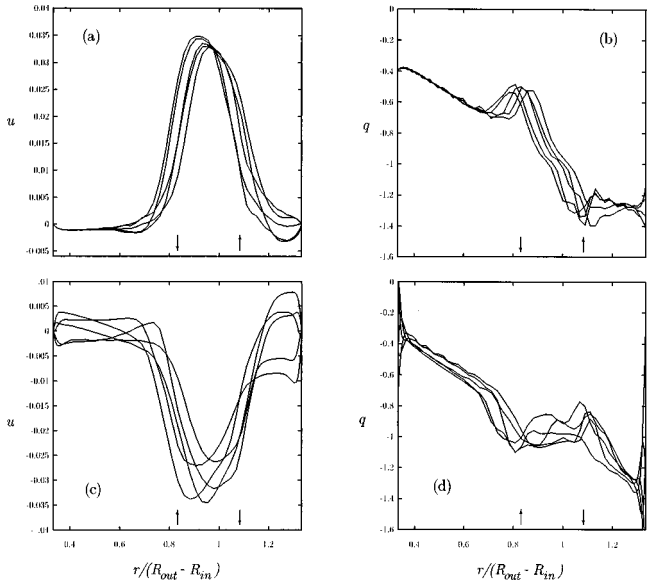


FIG. 7. (a) $u(r,\phi=\phi_j,t)$ and (b) $q(r,\phi=\phi_j,t)$ at fixed $t$ for the numerically computed locked eastward jet in fig. 4. Each of the five curves is for a fixed $\phi$, $\phi_j \equiv 2j\pi/5$, $j=1,\ldots,5$. Vertical arrows near the axis are as in fig. 6. (c) and (d) are the same as (a) and (b) but for the westward jet in fig. 5. The $u$ is plotted in units of $\beta(R_{out}-R_{in})^2$ and the $q$ in $\beta(R_{out}-R_{in})$. The locked eastward jet has one sharp gradient in $q$, and the linked westward jet has two with a flat region, indicating strong $q$ mixing. Due to $\nu$ and the vortices, the asymmetry between the eastward (a) and westward (c) jets are barely apparent. Contour plots of $q$ or $\psi$ in the $(r,\phi)$ plane are much more useful for displaying the asymmetry and for distinguishing the locked from the unlocked eastward jets (c.f., figs. 11 and 12). Unfortunately contour plots of $\psi$ and $q$ are not readily available from laboratory or planetary data.

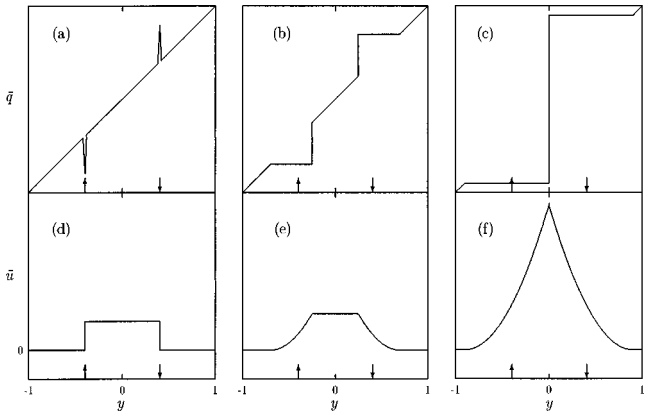


FIG. 8. Eastward jet model: a) $\overline{q}(y)$ for the primary flow, equations (11)–(12); b) $\overline{q}(y)$ at higher $P$ for the unlocked jet, equations (16)–(17); c) $\overline{q}(y)$ at still higher $P$ for the locked jet, equations (18)–(19); d), e), and f) are the $\overline{u}(y)$ corresponding to a), b), and c), respectively. Vertical arrows are as in fig. 6.

## IV. FLOW MODEL

Figure 7 is the numerically calculated flow at $P=44 \simeq 2P_{crit}$. (All units are CGS unless otherwise specified.) The $u$ does not look like $\overline{u}$ in equation (9), indicating vortex chains are present and the flow can no longer be approximated as a perturbation of the primary flow. Here we present our model of the mean secondary flow. The model is based on our experiences with high Reynolds number, barotropic flows on a $\beta$-plane[19,20] which show that: (1) regions where flows are well mixed tend to have nearly uniform values of $q$; (2) discontinuities or rapid changes in $q$ form at the interfaces of these regions, but discontinuities in **U** are rare; and (3) vortices embedded in turbulent flows are most robust when the surrounding flow has nearly uniform $q$ and always have the same sign of $\omega$ as the shear of the local jet. In these cases the vortices have little interaction with the surrounding flow, and because $Dq/Dt \simeq 0$, compact potential vortices advect with the local flow velocity. Incorporating these observations, the model has (1) a continuous $\overline{U}$ and discontinuous $\overline{q}(r)$, (2) Rossby waves that travel along discontinuities and make them wavy, and (3) vortices embedded in regions where $\overline{q}$ is uniform. We note that flow models with piecewise constant $q$ have been used previously. However, the motivation has usually been that the model permits the flow's dynamics to be computed analytically or with contour dynamics.[21,22] Here, our motivation is how the homogenization of $q$ progresses as the forcing is increased, and the model consists of both homogenized and undisturbed regions of $q$.

The component of our model flow written with the overbar represents the mean flow (averaged in $\phi$ or $t$) with $\overline{v}=0$. The $\overline{q}(y)$ and $\overline{u}(y)$ of the model are in figs. 8 and 9. In figs. 8b, 8e, 9b, and 9e the primary flow has become unstable and the flow contains waves and vortices. The mixing of $q$ near the slits causes the delta functions in the primary flow's $\overline{q}$ in figs. 8a and 9a to broaden which smoothes the discontinuities in $\overline{u}(y)$. The model's main feature and the reason that eastward and westward jets differ is this: As the delta functions broaden into smooth peaks, the sides of the peaks that are closer to $y=0$ have larger (smaller) jumps in $\overline{q}$ than the sides farther from $y=0$ for eastward (westward) jets. Figures 8b and 9b accentuate this by representing the peaks as flat-topped functions so that $\overline{q}$ is constant for $(Y_2^{slit}-a) \leqslant |y| \leqslant (Y_2^{slit}+b)$. For the eastward jet there are jumps in $\overline{q}$

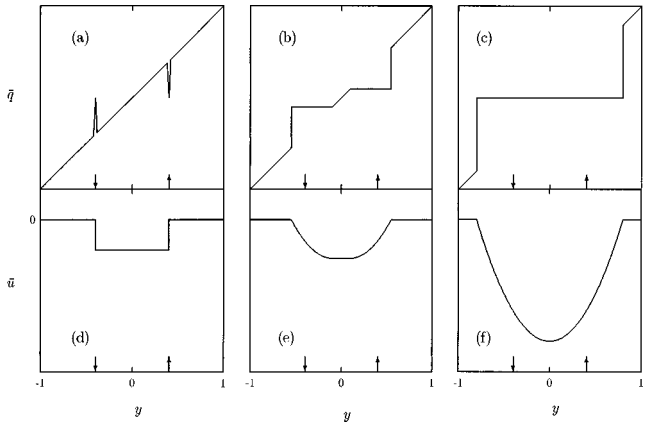


FIG. 9. Westward jet model: (a) $\overline{q}(y)$ for the primary flow, equations (11)–(12); (b) $\overline{q}(y)$ at higher $P$ where the two regions of uniform $\overline{q}$ are not linked together, equations (20)–(21); (c) $\overline{q}(y)$ at still higher $P$ where the two regions of uniform $\overline{q}$ are linked together, equations (22)–(24); (d), (e), and (f) are the $\overline{u}(y)$ corresponding to (a), (b), and (c), respectively. Vertical arrows near the $y$-axis are as in fig. 8.

Downloaded 12 Jul 2011 to 169.229.32.136. Redistribution subject to AIP license or copyright; see http://pof.aip.org/about/rights_and_permissions

of $\Delta\overline{q}=\beta(a+b)$ at $y=\pm(Y_2^{slit}-a)$, and elsewhere $\overline{q}$ is continuous. For the westward jet $\Delta\overline{q}=\beta(a+b)$, but the jumps are at $y=\pm(Y_2^{slit}+b)$. Physically, this model corresponds to mixing with homogenization of $q$ for $(Y_2^{slit}-a)\leqslant|y|\leqslant(Y_2^{slit}+b)$. In all other regions there are no waves or vortices, so $\overline{q}(y)$ is unchanged from its values in figs. 8a and 9a. The $\overline{u}(y)$, $a$ and $b$ are determined by noting that the integral of equation (2) (in Cartesian coordinates) over all $x$ and $t$ and over $-(Y_2^{slit}+b^+)\leqslant y\leqslant(Y_2^{slit}+b^+)$ (where $b^+$ is the limit of $y$ approaching $b$ from the positive direction) requires:

$$\int_{-(Y_2^{slit}+b^+)}^{Y_2^{slit}+b^+}\overline{u}(y')dy'=\pm 2V_0Y_2^{slit}, \tag{14}$$

where the upper (lower) sign is for the eastward (westward) jet. In addition, an integral of equation (4) gives

$$\int_0^{Y_2^{slit}+b^+}\overline{\omega}(y')dy'=\pm V_0, \tag{15}$$

where the sign convention in equation (14) is used. Equation (15) is valid only when there is no vorticity transport across the $y=0$ as would be expected for the flows in figs. 8b and 9b.

### A. Eastward jet model

For the eastward jet in figs. 8b and 8e equations (14) and (15) give:

$$a=\frac{1}{3}\sqrt{\frac{2V_0}{\beta}};\quad b=2a;\quad \Delta\overline{q}\equiv\beta(a+b)=\sqrt{2\beta V_0} \tag{16}$$

$$\overline{u}(y)=\begin{cases}0 & \text{for } |y|>(Y_2^{slit}+b),\\ \beta(|y|-Y_2^{slit}-b)^2/2 & \\ \quad\text{for } (Y_2^{slit}+b)\geqslant|y|\geqslant(Y_2^{slit}-a),\\ V_0\equiv f\tau\mathscr{P}/H & \text{for } (Y_2^{slit}-a)>|y|.\end{cases} \tag{17}$$

In figs. 8b and 8e in the regions $(Y_2^{slit}-a)>|y|$ and $|y|>(Y_2^{slit}+b)$, neither $\overline{q}(y)$ nor $\overline{u}(y)$ are changed from their primary values. For $\mathscr{P}\geqslant\mathscr{P}_{east}^{link}\equiv 9\beta H(Y_2^{slit}-Y_1^{slit})^2/8f\tau$, the two mixed regions of uniform $\overline{q}$ become so large that they touch each other, and the flow looks like figs. 8c and 8f with $a\equiv Y_2^{slit}$. The two jumps in $\overline{q}$ merge together, the value of $\Delta\overline{q}$ doubles, and $\overline{u}(y)$ develops a cusp at $y=0$. After the merger the flow retains the appearance of figs. 8c and 8f with $\overline{u}(y)$ still given by (17) and

$$a\equiv Y_2^{slit},\quad b=|Y_2^{slit}-Y_1^{slit}|[3(\mathscr{P}/\mathscr{P}_{east}^{link})^{1/3}-1]/2,$$

$$\Delta\overline{q}=2\beta(b+a), \tag{18}$$

$$\overline{u}(0)=\beta(b+Y_2^{slit})^2/2=V_0(\mathscr{P}_{east}^{link}/\mathscr{P})^{1/3}. \tag{19}$$

Note that for $\mathscr{P}>\mathscr{P}_{east}^{link}$ equation (15) is not used because it is invalid; the flow in figs 8c and 8f transport vorticity across the $y=0$ line, or in other words, the opposite-signed vortex layers at the two slits partially annihilate each other. (*n.b.*, the momenta created by the forcing at the two slits have the same sign and do not annihilate each other.)

### B. Westward jet model

At small $\mathscr{P}$ the westward jet changes from the primary flow in figs. 9a and 9d to the forms in figs. 9b and 9e with

$$a=\frac{2}{3}\sqrt{\frac{2V_0}{\beta}};\quad b=a/2;\quad \Delta\overline{q}\equiv\beta(a+b)=\sqrt{2\beta V_0} \tag{20}$$

$$\overline{u}(y)=\begin{cases}0 & \text{for } |y|>(Y_2^{slit}+b),\\ \beta[(|y|-Y_2^{slit}+a)^2-(a+b)^2]/2 & \\ \quad\text{for } (Y_2^{slit}+b)\geqslant|y|\geqslant(Y_2^{slit}-a),\\ -V_0\equiv-f\tau\mathscr{P}/H & \text{for } (Y_2^{slit}-a)>|y|.\end{cases} \tag{21}$$

For $\mathscr{P}\geqslant\mathscr{P}_{west}^{link}\equiv 9\beta H(Y_2^{slit}-Y_1^{slit})^2/32f\tau$, the two regions of uniform $\overline{q}$ are linked together, and the flow looks like figs. 9c and 9f with $a=Y_2^{slit}$. However, unlike the eastward jet, the two jumps in $\overline{q}$ do not merge together and there is never a cusp in $\overline{u}(y)$ at $y=0$. In figs. 9c and 9f $\overline{u}(y)$ is given by (21), $a\equiv Y_2^{slit}$ (equation (15) is not used because it is invalid), and

$$b=|Y_2^{slit}-Y_1^{slit}|[\tfrac{3}{2}(\mathscr{P}/\mathscr{P}_{west}^{link})^{1/3}-1]/2, \tag{22}$$

$$\Delta\overline{q}=\beta(b+a), \tag{23}$$

$$\overline{u}(0)=-\beta(b+Y_2^{slit})^2/2=-V_0(\mathscr{P}_{west}^{link}/\mathscr{P})^{1/3}. \tag{24}$$

### C. Rossby waves and vortices

We expect differences between $\overline{u}$ and the laboratory (or numerically computed) **U** because the latter is filled with vortices and Rossby waves. Rossby waves require gradients in $q$, so the model Rossby waves are centered at the discontinuities of $\overline{q}$ and cause the locations of the discontinuities to meander in $y$ (or $r$) as a function of $x$ (or $\phi$). Eigenmodes of the Cartesian form of equation (2) are proportional to $e^{ik(x-ct)}$ and obey the Rayleigh–Kuo equation with matching conditions at discontinuities.[23] The eigenmodes (computed with $\nu=1/\tau=0$) of $\overline{u}(y)$ are neutrally stable, so $Imag(\overline{c})=0$, (using the overbar on $c$ to denote that it is associated with our model) and *for all of our model flows:*

$$\overline{c}=\overline{u}(y_d)-\frac{\chi\beta(a+b)}{2k}, \tag{25}$$

where $y_d$ is the location of the discontinuity in $\overline{q}(y)$ (i.e., $y_d\equiv\pm(Y_2^{slit}-a)$ for the eastward, and $y_d\equiv\pm(Y_2^{slit}+b)$ for the westward jets). The dimensionless number $\chi>0$, is order unity, and easily found to be the solutions of transcendental equations.[24,25] For eastward jets with one discontinuity (at $y_d=0$), $\chi=2$, so equation (25) becomes *for eastward jets with one discontinuity:*

$$\overline{c}=\overline{u}(0)-\frac{\Delta\overline{q}}{2k}. \tag{26}$$

For eastward jets with two discontinuities and all westward jets, $\Delta\overline{q}=\beta(a+b)$. In the limits that $2k(Y_2^{slit}-a)\gg 1$ and $2k(a+b)\gg 1$, $\chi\simeq(1-(1)/(2k(a+b))^{-1}$, so for these limits *for eastward jets with two discontinuities and all westward jets:*

Downloaded 12 Jul 2011 to 169.229.32.136. Redistribution subject to AIP license or copyright; see http://pof.aip.org/about/rights_and_permissions

$$\overline{c} \simeq \overline{u}(y_d) - \frac{\Delta\overline{q}}{2k}\left(1 - \frac{1}{2k(a+b)}\right)^{-1}. \tag{27}$$

Equation (25) shows why westward jets have $c<0$: $u(y_d)=0$, $\beta>0$ and $\chi>0$. For eastward jets $u(y_d)=V_0>0$, so $c$ can be (and is) positive. Another reason why the signs of $c_i$ differ for eastward and westward jets is that the Rossby waves in these flows advect at the same speed as their accompanying vortex chains and vortices advect with the local velocity of the flow—see below—which is always positive (negative) for the eastward (westward) model flow.

To see qualitatively why the $c_i$ decrease when the eastward jet's discontinuities merge, compare equation (26) with (27), and note that when the discontinuities merge, $\Delta\overline{q}$ suddenly doubles, while $y_d$ smoothly goes to zero and $1/2k(a+b)$ remains small. To understand the decrease in $c_i$ quantitatively, use equation (25) and the fact that the governing equation[24] for $\chi$ along with equations (13) and (16) show that for $0 \leqslant (\mathscr{P}_{east}^{link} - \mathscr{P}) \ll \mathscr{P}_{east}^{link}$

$$\chi \simeq 1 + e^{-(kY_2^{slit})(\mathscr{P}_{east}^{link} - \mathscr{P})/\mathscr{P}_{east}^{link}}. \tag{28}$$

Because $kY_2^{slit}$ is large, $\chi$ rapidly changes from 1 to 2 as $\mathscr{P} \to \mathscr{P}_{east}^{link}$ (and the two discontinuities of the eastward jet merge into one). Note that $\chi$ remains 2 for $\mathscr{P} > \mathscr{P}_{east}^{link}$.

In our model[26] the Rossby eigenmode is exponentially peaked at the discontinuity in $\overline{q}$ located at $y=y_d + Ae^{ik(x-ct)}$, where $A$ is the Rossby wave amplitude. In our numerically calculated flows (c.f., fig. 4), the Rossby wave is visible as a deformation of the contours of constant $q$ and in particular of the contour where $|\nabla q|$ is greatest. As the Rossby waves of the westward jets move closer to the annular boundaries, they become less pronounced. Each Rossby wave is also associated with an entrained vortex chain with the vortices riding along at the Rossby wave speed. Because vortices tend to lie in regions of nearly uniform $q$, their locations, $y^*$, satisfy the inequality $Y_2^{slit} + b > |y^*| > Y_2^{slit} - a$. For westward jets in which the two regions of constant $\overline{q}$ are joined together (as in fig. 9f), the two chains of vortices often overlap in $y$, so they can strongly interact with each other (fig. 5). However in the eastward jets, the two regions of uniform $q$ are physically separated from each other by one or two jumps of potential vorticity. Thus, the two vortex chains in the eastward flow only weakly interact with each other. Because vortices embedded in east–west flows of uniform $q$ advect approximately with the local velocity[20] and because the waves and vortices have the same speed, $y^*$ satisfies $\overline{u}(y^*) \simeq \overline{c}$, where $\overline{u}(y^*)$ is given by equation (17) or (21). This constrains the allowable values of $k$ to:

$$k \geqslant \chi\beta(a+b)/2|\overline{u}(0)|. \tag{29}$$

## V. TESTS OF THE MODEL

To compare *directly* the $\overline{u}$ of the model with the laboratory experiment's velocity is difficult because the model's discontinuities in $q$ are smoothed by $\nu$ (which is not in the model). Moreover as we show below, the laboratory (and numerically computed) flows averaged over $\phi$ are deceptive in appearance. It is better to compare the locations and speeds of the vortices and waves, the locking of the Rossby waves, and the flow's hysteresis. The difficulties in comparing the model and laboratory flows are illustrated in fig. 10 which shows a laboratory five-fold symmetric eastward jet similar to the numerically computed seven-fold flow (fig. 4). The $u(r)$ in fig. 10a has been averaged over $\phi$ (as was the planetary $u$ in fig. 1). The averaged laboratory flow looks like a Bickley jet (i.e., proportional to $\mathrm{sech}^2(r/L_{Bick})$ for some length $L_{Bick}$—see section VI) with no discontinuity in $q(r)$ or in the slope of $u(r)$. The meandering Rossby wave wipes out any signature of the discontinuity in the averaged flow. Figure 10b shows the $u(r,\phi,t)$ of the same flow in fig. 10a at a fixed $t$ and at two fixed values of $\phi$. Figure 10b looks like the model in fig. 8f whose hallmark is the *discontinuity* in the slope of $u$ at its peak with the modification that the Rossby wave makes the discontinuity (and location of the peak velocity) of the laboratory flow wavy in $\phi$. Figure 10b quantitatively supports our model of a locked eastward jet which predicts that the width of the jet (the length in $r$ in fig. 10b over which the $u$ is non-zero) or $(a_1+a_2+b_1+b_2)$ is related to $\Delta[\partial u/\partial r]$ which is defined to be the value of the discontinuity in the slope of $u$: $-\Delta[\partial u/\partial r] = \Delta\overline{q} = \beta(a_1+a_2+b_1+b_2)$. Using $(a_1+a_2+b_1+b_2) \simeq 20$ cm from fig. 10b and the laboratory value of $\beta = 0.135\ \mathrm{cm}^{-1}\,\mathrm{s}^{-1}$ gives $-\Delta[\partial u/\partial r] \simeq 2.7$. The values of $-\Delta[\partial u/\partial r]$ in fig. 10b are $\sim 3.0$ and $\sim 2.0$ for the solid and dotted curves, respectively. Unfortunately, other than fig. 10b, there is little other laboratory data (and no reliable planetary data) for non-averaged values of $u(r,\phi,t)$, so *direct* comparisons with the model are difficult.

The model, laboratory, and numerically computed flows all have hysteresis. For $\mathscr{P} \geqslant \mathscr{P}_{east}^{link}$ (or $\mathscr{P} \geqslant \mathscr{P}_{west}^{link}$) the model flows must look like fig. 8f (or 9f). However, for smaller values of $\mathscr{P}$ the flows look either like fig. 8f (or 9f) or like fig. 8e (or 9e) subject to the constraint that $b \geqslant 0$. Thus there is a range of $\mathscr{P}$ where both model flows can exist. For the same $\mathscr{P}$, the energy of the flows in figs. 8f and 9f are greater than those of the flows in figs. 8e and 9e. To determine where the model eastward flow has hysteresis, let the distance between the two discontinuities in $\overline{q}(y)$ be $L_{sep} \equiv (Y_2^{slit} - Y_1^{slit} - 2a)$. $L_{sep}$ decreases with increasing $\mathscr{P}$ and is zero when $\mathscr{P} = \mathscr{P}_{east}^{link}$. We expect the two Rossby waves, centered on the discontinuities, to merge and lock together due to non-linearities when $kL_{sep} \lesssim 1$ where $k$ is the average Rossby wavenumber. This means that there should be hysteresis between locked and unlocked states when $\mathscr{P} < \mathscr{P}_{east}^{link}$ and $kL_{sep} \lesssim 1$. This has been verified by the numerical solutions of equations (2)–(3): For $P \leqslant 28$ the eastward flow is temporally quasi-periodic, unlocked, and of the form of equation (1). For $P \geqslant 36$ flows are locked (although if $P$ becomes too large, new instabilities occur).[18] For a small range near $P=32$ the flows are hysteretic with $m_1 \simeq m_2 \simeq 9$, so that $kL_{sep} = 0.904$, consistent with the model when we set $k = m_i/R_i^{slit}$. The laboratory eastward jets[3] behave similarly to our numerical solutions except the range of $P$ where the flow is hysteretic is $\sim 22$.

The main prediction of our model is that the eastward jet at low $P$ (fig. 8b) and the westward jet at low and high $P$ (in figs. 9b and 9c) have two discontinuities in $\overline{q}$, and each acts as a Rossby wave guide. Each discontinuity has an associ-

Downloaded 12 Jul 2011 to 169.229.32.136. Redistribution subject to AIP license or copyright; see http://pof.aip.org/about/rights_and_permissions

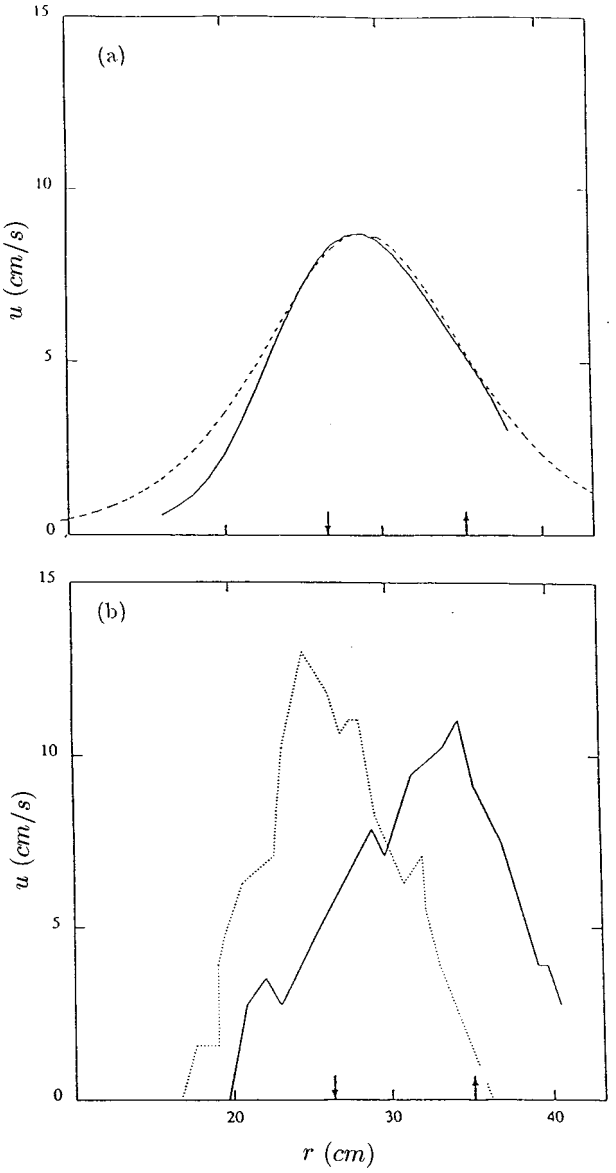


FIG. 10. (a) Azimuthally averaged value (solid curve) and the fit to a sech$^2$ function (dotted curve) of $u(r,\phi,t)$ at fixed $t$ for an eastward jet at $P=100$ and $f=25.2$ (from Sommeria *et al.*,[1] fig. 4, with permission). (b) The same $u(r,\phi,t)$ at fixed $t$ and at two different values of $\phi$. The solid (dotted) curve is for the value of $\phi$ where the jet is closest to the outer (inner) boundary.

ated vortex chain that advects azimuthally at the Rossby wave's speed. In an annular geometry the strengths of the two discontinuities differ, so the wave speeds differ, and the chains are unlocked. For sufficiently large $P$, the eastward jet's two discontinuities merge into a single large one, there is only one Rossby wave, both vortex chains move at that speed, and the flow is locked. The model does not predict that the westward jet's vortex chains lock. We have found that this scenario is consistent with all of our numerical calculations. We now show that there is also quantitative agreement between our model and numerical calculations.

### A. Eastward jets

Tables I and II compare the Cartesian model's values of $c_1$ predicted by equation (25) with the wave speeds of the numerically computed solutions of equation (2) in annular geometry. Also shown are comparisons of $\overline{\Omega}_1$ which is defined to be $\overline{u}(r)/r$ evaluated at the discontinuity associated with $R_1^{slit}$. Agreement is good. The tables were computed by imposing an $m$-fold symmetry so $m_1=m_2$. With no imposed symmetry, the flow at $P=28$ (fig. 11) was unlocked with $m_1=m_2=12$ (as were flows at $P=18$ and $P=24$) independent of the initial conditions (that we tried). When no symmetry was imposed at $P=44$, the final flow is locked and independent of initial conditions with $m_2=7$ and $7\leqslant m_1\leqslant 9$. The value of $m_1$ depended on $L^{slit}$ (see the Appendix) and decreases with increasing thickness. The most interesting feature of the eastward jet model is that $\overline{c_1}$ and $\overline{c_2}$ abruptly decrease when they lock. Equations (25) and (26) with $k_i(\overline{u_i}-\overline{c_i})$ replaced with $m_i(\overline{\Omega}_i-\overline{c_i})$ show that this decrease is $\sim\Delta\overline{q_i}/2m_i$. We have tested this prediction in two ways. When both locked and unlocked eastward jets exist at the same $P$, equation (13) with $\mathscr{P}$ replaced with $P/2\pi R_i^{slit}$ and equations (16)–(18) show that this decrease is given by

$$[m_1(\overline{\Omega}_1-\overline{c_1})]^{\text{locked}}/[m_1(\overline{\Omega}_1-\overline{c_1})]^{\text{unlocked}} = 2(P_{east}^{link}/P)^{1/6}/\chi_1. \tag{30}$$

(For locked flows, we use the subscript 1 to mean 1 *and* 2.) For $P=32$ the right-side of equation (30) computed with the model at the parameter values used in Table II is 1.45, while the ratio on the left-hand side determined from the numerical solution of equations (2)–(3) with $m_1=m_2=9$ is 1.56—a difference of only 7%. Because the model is Cartesian and the numerical calculation is annular, we cannot expect them to agree to much better than $(a_1+b_1)/\pi R_1^{slit}$ or $\sim 10\%$ at $P=32$, so an error of 7% is very good. The model predicts that locking is accompanied by the merger of two discontinuities in $q$, and we note that the numerical simulations show that $\Delta q_1$ of the locked flow is more than twice as big as that

TABLE I. For an unlocked eastward jet at $P=28$, the comparison between our model (quantities with overbar) and the numerically computed solutions with $m_1=m_2$ (no overbar). We use[15] $\nu=0.033$, $f=6\pi$, $L^{slit}=1.2$ (see the Appendix), and $R_1^{slit}=27.0$. The model has $(a_1+b_1)=7.44$, $\overline{\Omega}_1=0.0947\beta(R_{out}-R_{in})$, and $\Delta\overline{q}_1=0.750\beta(R_{out}-R_{in})$. (All dimensional numbers have CGS units.) In practice it is difficult to determine the value of $u$ at the ''discontinuity'' in the numerically computed flows—see fig. 7—so we define $\Omega_1$ to be the maximum value of the computed flow's $u(r,\phi,t)/r$. Agreement in $c_1$ improves as $m_1$ increases because the differences between the Cartesian and annular geometry decrease. By setting $k=m_i/R_i^{slit}$, $P=2\pi R_i^{slit}\mathscr{P}_i$ and replacing $\overline{u}(y_d)$ with $\overline{\Omega}_i$, equation (25) in an annular geometry becomes $2m_1(\overline{\Omega}_1-\overline{c_1})=\chi_1\beta(a_1+b_1)$. The computed flows' values of $2m_1(\Omega_1-c_1)$ are only weakly dependent on $m_1$ because equation (25) shows that they are proportional to $\chi_1$ which only weakly depends on $m_1$. According to equation (35) the ratio in the last column would be unity if the flow were a Bickley jet. In equation (35) we set $R\equiv(R_1^{slit}+R_2^{slit})/2$.

| $m_1$ | $\Omega_1/\overline{\Omega}_1$ | $\frac{(\Omega_1-c_1)}{(\overline{\Omega}_1-\overline{c_1})}$ | $\frac{2m_1(\Omega_1-c_1)}{\beta(R_{out}-R_{in})}$ | $\frac{c_1}{\beta(R_{out}-R_{in})}$ | $\frac{2\Omega_1/3-c_1}{\beta R/m_1^2}$ |
|---|---|---|---|---|---|
| 9 | 0.849 | 0.728 | 0.885 | 0.0311 | 0.581 |
| 10 | 0.818 | 0.760 | 0.895 | 0.0327 | 0.605 |
| 11 | 0.821 | 0.854 | 0.974 | 0.0336 | 0.703 |
| 12 | 0.821 | 0.927 | 1.026 | 0.0350 | 0.776 |
| 13 | 0.831 | 1.036 | 1.111 | 0.0359 | 0.893 |

Downloaded 12 Jul 2011 to 169.229.32.136. Redistribution subject to AIP license or copyright; see http://pof.aip.org/about/rights_and_permissions

TABLE II. Same as Table I but for the locked eastward jet at $P=44$ with $m_2=m_1$. For each $m_1$, the model gives $(a_1+b_1)=10.18$, $\overline{\Omega}_i=0.168\beta(R_{out}-R_{in})$, $(a_2+b_2)=9.33$, and $\Delta\overline{q}_i\equiv 2m_i(\overline{\Omega}_i-\overline{c}_i)=1.97\beta(R_{out}-R_{in})$. (Because the flow is locked, the subscript $i$ means 1 and 2.) All dimensional numbers have CGS units. The model overestimates $\Omega_i$ and $\Delta q_i$ (although its prediction that $\Omega_i$ is independent of $m_1$ is consistent with the numerical calculations) because the model flow is not smoothed by $\nu$ or by vortices. The overestimates are worse when there is strong radial mixing, as is the case at $P=44$ for the low $m$ (large area) vortex chains. The values of $\Delta q_1$ (inferred from the values of $2m_1(\Omega_1-c_1)$ in Tables I and II) are approximately twice as large for the locked flows at $P=44$ as they are for the unlocked flows at $P=28$. For locked flows, equation (26) predicts that $2m_i(\overline{\Omega}_i-\overline{c}_i)=\Delta\overline{q}_i$ and should therefore be independent of $m_i$. However, for the computed flows, this quantity slowly increases with $m_i$ because in real flows the largest diameter vortices (those with lowest $m$) spread the ''discontinuity'' over the largest radial distance. A large spread creates a small change in slope of the velocity across the ''discontinuity'' which in turn causes a small value of $\Delta q_i=2m_i(\Omega_i-c_i)$. The last column shows that $(2\Omega_1/3-c_1)$ does not scale as $m_1^{-2}$ as predicted by the Bickley jet model.

| $m_1$ | $\Omega_i/\overline{\Omega}_i$ | $\frac{(\Omega_i-c_i)}{(\overline{\Omega}_i-\overline{c}_i)}$ | $\frac{2m_i(\Omega_i-c_i)}{\beta(R_{out}-R_{in})}$ | $\frac{c_i}{\beta(R_{out}-R_{in})}$ | $\frac{2\Omega_1/3-c_1}{\beta R/m_1^2}$ |
|---|---|---|---|---|---|
| 7 | 0.696 | 0.779 | 1.53 | 0.0080 | 1.05 |
| 8 | 0.724 | 0.865 | 1.70 | 0.0159 | 1.34 |
| 9 | 0.731 | 0.921 | 1.81 | 0.0224 | 1.54 |
| 10 | 0.737 | 0.983 | 1.93 | 0.0274 | 1.77 |
| 11 | 0.735 | 1.04 | 2.05 | 0.0308 | 2.00 |
| 12 | 0.741 | 1.12 | 2.20 | 0.0332 | 2.30 |

of the unlocked flow. (The locked jet's larger value of $(a_1+b_1)$ also contributes to the increase in $\Delta q_1$.) For the same control parameters as in Table II, there is also a stable, locked flow with $m_1=11$ and $m_2=9$ (fig. 12). This flow agrees with equation (30) to within 10%. Equation (30) is a good test of the model because $(\Omega_i-c_i)$ varies greatly with $m_i$ and $P$. We have also carried out initial-value calculations

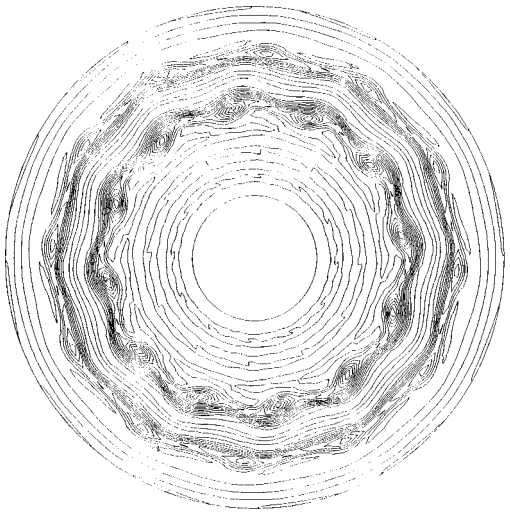

FIG. 11. $q$ of the numerically computed[15] unlocked eastward jet at $P=28$, $f=6\pi$, $\nu=0.033$, $R_1^{slit}=27.0$, and $m_1=m_2=12$. The two regions of uniform $q$ are not linked together, so the two chains are separated by two near discontinuities in $q$, and the flow looks like the model in figs. 8b and 8e. The vortices in the chain at smaller $r$ have $\omega>0$, while those at greater $r$ have $\omega<0$.

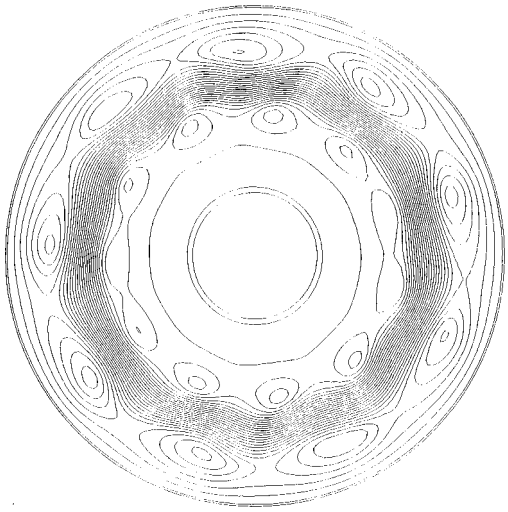

FIG. 12. Stream function of the numerically computed,[15] locked, eastward jet at $P=32$, $f=6\pi$, $\nu=0.033$, $R_1^{slit}=27.0$, $m_1=11$, and $m_2=9$. Vortices in the chain at small $r$ have $\omega>0$; those at greater $r$ have $\omega<0$. It is not necessary for $m_1=m_2$ for the flow to lock (and to be steady in some rotating frame).

that mimic the laboratory experiments in which $P$ is abruptly increased: We start with an unlocked eastward jet in equilibrium at $P\leqslant 28$ and use it to initialize a calculation with $P\geqslant 36$. In these initial-value calculations, as in the experiments, $c_1$ and $c_2$ decrease by $\sim 50\%$ at the same time that they lock together.

Another feature of our model of locked eastward jets is that equation (29) constrains $m_1$ to $m_1\geqslant\Delta\overline{q}_1/2\overline{\Omega}_1$. At $P=44$, this requires $m_1>5.9$. Our numerical calculations are consistent with this: We could compute locked flows with $m>6$, but were unable to with $m\leqslant 6$. When 6-fold symmetry was imposed in our numerical calculation, the flow was quasi-periodic in time and oscillated between having 6 vortices and 12. Equation (29) is also consistent with laboratory experiments[1] at $P=44$ where flows with different values of $m_1$ were stable, but none with $m_1<6$. Equation (29) shows that the smallest allowable $m_i$ decreases with increasing $P$, and this has also been confirmed numerically and experimentally. None of our initial-value calculations have created solutions that violate equation (29).

In summary it should be noted that the $q$, **U**, and stream functions of the eastward jets in figs. 4, 7, 11, and 12 show many of our model's features. There are Rossby waves that peak in the layers where $q$ changes most rapidly (which for a locked flow is where the jet's velocity peaks). The two vortex chains are radially separated from each other and from the peaks of the Rossby waves. As fig. 4 shows, the vortices that make up the chains are often nestled in the troughs of the Rossby waves, and in all cases they travel along with them. The chains are located in the two regions of nearly uniform $q$ at $r_i^*$ such that $u(r_i^*,\phi,t)/r_i^*\simeq c_i$, and the chains are separated from each other by one (for the locked flow—figs. 4 and 12) or two (for the unlocked flow—fig. 11) approximate discontinuities in $q$.

Downloaded 12 Jul 2011 to 169.229.32.136. Redistribution subject to AIP license or copyright; see http://pof.aip.org/about/rights_and_permissions

TABLE III. Same as Table II but for the westward jet at $P=44$. For each $m_i$, $\Delta\overline{q_1}=0.815\beta(R_{out}-R_{in})$, $\Delta\overline{q_2}=0.747\beta(R_{out}-R_{in})$, $(a_1+b_1)=8.08$, and $(a_2+b_2)=7.41$. The value of $q_1$ does not double when the flow locks, as it does for the eastward jets. $\Delta q_2$ is lower than the values predicted by the model because the outer discontinuity has run into $R_{out}$ (which makes $\overline{c_2}$ uncomputable in our model). The last two columns show that the Bickley jet model in equation (35) does not work well either for $c_1$ or $c_2$.

| | $m_1$ | $m_2$ | $c_1/\overline{c_1}$ | $\frac{c_1}{\beta(R_{out}-R_{in})}$ | $\frac{c_2}{\beta(R_{out}-R_{in})}$ | $\frac{2\Omega_1/3-c_1}{\beta R/m_1^2}$ | $\frac{2\Omega_1/3-c_2}{\beta R/m_2^2}$ |
|---|---|---|---|---|---|---|---|
| unlocked | 7 | 6 | 1.16 | −0.0918 | −0.0748 | 0.374 | 0.079 |
| unlocked | 7 | 5 | 1.15 | −0.0908 | −0.0778 | 0.358 | 0.078 |
| locked | 8 | 4 | 1.29 | −0.0846 | −0.0846 | 0.342 | 0.086 |

### B. Westward jets

Because our model predicts that westward jets do not lock, we have tried very hard to make them lock and disprove our model. Of all our westward-flow, numerical calculations, locking occurred only in a small window[15] near $P=44$. Locking was obtained by adjusting $L^{slit}$ (whose effective value in the laboratory experiments is uncertain—see the Appendix) which changes the flows' $m_i$. The locked flow has $m_1=8$ and $m_2=4$ (fig. 5 and Table III). Unlike locked eastward jets, where the two Rossby waves and two discontinuities in $q$ merge into one, the locked westward jet still has two waves and two discontinuities. The **U** of the locked and unlocked westward jets look nearly the same; whereas, those of the locked and unlocked eastward jets differ. Unlike the initial-value calculations of the eastward jets, where $c_i$ suddenly decreases when the flow locks, there is almost no change in $c_i$ ( or $\Delta q_i$) of the westward jet when it locks. Our explanation is that the locked westward jet is a fluke: near $P=44$ the $c_1$ and $c_2$ of the two Rossby waves with $m_1=8$ and $m_2=4$ change slowly with $P$ but not at the same rate. It appears that their locking is just a matter of tuning $P$ until they are equal. For the flows in Table III, equations (22)–(25) give $\overline{c_i}\propto(R_i^{slit})^{-1/3}\chi_i/m_i$. Because $\chi_1\simeq\chi_2$, this suggests that in order for $c_1=c_2$ and the westward flow to lock that $m_1>m_2$ which is consistent[27] with Table III. Currently, it is uncertain whether the laboratory experiments have westward jets with locked vortex chains.[28]

Another important result shown in Tables III and IV is that the westward jets have $c_i<0$ (opposite in sign to the eastward jets) in accord with the model. Moreover, the model predicts that the characteristic difference in value between the $c_i$ of the eastward and westward jets is the order of the characteristic value of the $\Omega_i$ of an eastward jet. This is consistent with Tables I–IV. Figures 5 and 7 show the $q$, **U** and stream functions of westward jets. Like the model, they show that the westward jets are broader, less peaked, and less wavy than the eastward jets, and that the two vortex chains of the former are radially closer together than those of the latter. For $P=44$ they are intertwined with each other.

## VI. BICKLEY JET MODEL

We have shown how well our model, based on the homogenization of $q$, agrees with the experiments and simulations. Here we review the Bickley jet model[2,3,12] and summarize its shortcomings. A Bickley jet has a velocity $u(y\equiv U_0\mathrm{sech}^2(y/L_{Bick})$ where $U_0$ and $L_{Bick}$ are unknown parameters. The Bickley model was motivated by fig. 10a which shows that the *azimuthal average* of the laboratory flow's $u(r,\phi,t)$ at fixed $t$ fits a sech$^2$. Momentum balance (or integrating equation (2) in Cartesian coordinates as we did to obtain equation (14)) relates $U_0$ to the pumping rate $\mathscr{P}$:

$$U_0=f\tau\mathscr{P}|Y_2^{slit}-Y_1^{slit}|/2HL_{Bick}. \tag{31}$$

Unlike the jets in our model which are always neutrally stable, the eastward Bickley jet is unstable when 0

TABLE IV. Same as Table III but for the unlocked westward jet at $P=30$ with $m_2=m_1$. For each $m$ the model gives $\Delta\overline{q_1}=0.717\beta(R_{out}-R_{in})$, $\Delta\overline{q_2}=0.657\beta(R_{out}-R_{in})$, $(a_1+b_1)=7.12$, and $(a_2+b_2)=6.52$. The differences between $\overline{c_i}$ and $c_i$ in Tables III and IV are mostly due to interactions between the two vortex chains which are much closer together for the westward than the eastward jets (especially for the locked westward jet).[29] The westward jet's outer vortex chain, centered at $r=r_2^*$, has $\omega>0$, while the inner chain has $\omega<0$. Thus, the velocity created by vortices in the outer chain pushes fluid at $r<r_2^*$ (as well as the inner vortex chain) in the $-\phi$ direction. Similarly, the inner vortex chain pushes the outer chain in the $-\phi$ direction. Because the $c_i$ of the waves of the westward jet are also negative, $|c_i|$ is greater than $|\overline{c_i}|$. Because $r_2^*$ is close to $R_{out}$, the outer chain's image created by the outer boundary is strong. The image, which has $\omega<0$, advects the outer chain in the $+\phi$ direction which cancels, somewhat, the effects of the inner vortex chain. Thus $c_2/\overline{c_2}\simeq 1$.

| $m_1$ | $c_1/\overline{c_1}$ | $c_2/\overline{c_2}$ | $\frac{c_1}{\beta(R_{out}-R_{in})}$ | $\frac{c_2}{\beta(R_{out}-R_{in})}$ | $\frac{2\Omega_1/3-c_1}{\beta R/m_1^2}$ | $\frac{2\Omega_1/3-c_2}{\beta R/m_2^2}$ |
|---|---|---|---|---|---|---|
| 7 | 1.00 | 0.717 | −0.0728 | −0.0559 | 0.227 | −0.039 |
| 8 | 1.140 | 0.853 | −0.0689 | −0.0536 | 0.216 | −0.098 |
| 9 | 1.280 | 0.962 | −0.0663 | −0.0506 | 0.206 | −0.200 |
| 10 | 1.42 | 1.06 | −0.0640 | −0.0480 | 0.181 | −0.331 |

Downloaded 12 Jul 2011 to 169.229.32.136. Redistribution subject to AIP license or copyright; see http://pof.aip.org/about/rights_and_permissions

$<\beta L_{Bick}^2/U_0<2/3$. At large $P$ it was argued[1,2] that instabilities would increase $L_{Bick}$ until the jet is marginally stable (i.e., no growing modes for *any* azimuthal wavenumber), which for eastward jets requires

$$\beta L_{Bick}^2/U_0=2/3. \tag{32}$$

This jet has one neutrally stable, non-singular eigenmode. It has wave speed[1] and azimuthal wavenumber

$$c_{m.s.}=\Omega_1/3, \quad m_{m.s.}=\sqrt{2}R/L_{Bick}, \tag{33}$$

where $R$ is the mean $r$ of the jet and where $\Omega_1$ for this model is defined as $U_0/R$. Sommeria *et al.*[2] found experimental values of $m_i$ that were similar to, but consistently smaller than $m_{m.s.}$. They also reported values of $U_0$ and $U_0^{theory} \equiv [3(f\tau\mathscr{P})^2\beta(R_2^{slit}-R_1^{slit})^2/H^2]^{1/3}/2$ as functions of $(Pf)$ in order to validate the Bickley jet model, where $U_0^{theory}$ is the solution to equations (31) and (32). We can use this same data to test their assumption that the jet is marginally stable (without knowing $L_{Bick}$ whose experimental values were not published). Define $\alpha$ such that $\alpha \equiv 3\beta L_{Bick}^2/2U_0$. Comparison of this definition with equation (32) shows that $\alpha$ measures how close the jet is to marginally stable. By definition of $\alpha$ and the assumption that the experimentally-obtained values of $U_0$ and $L_{Bick}$ satisfy equation (31) (whose validity relies only on the conservation of momentum) gives $\alpha=(U_0^{theory}/U_0)^3$. For large values of $(Pf)$ (e.g., 8000, where the marginally stable assumption should work best), the experimental values give $\alpha \simeq 0.5$, so the jet is not marginal. The Bickley jet model's prediction that $c_i=c_{m.s.}=\Omega_1/3$ cannot be tested experimentally at large $P$ because the flow is chaotic and finding $c_i$ is ambiguous. However, our numerical calculations at $P=64$ give $c_1 \simeq 0.12\Omega_1$ (and shows that $c_1$ decreases with increasing $P$) which disagrees with the Bickley model. For $P<65$, Solomon *et al.*[3] used the eastward Bickley jet model without the assumption of marginal stability, so $0<\beta L_{Bick}^2/U_0<2/3$. For these non-marginal Bickley jets there are two neutral, regular, sinuous Rossby waves with speeds $c_\pm$ and wavenumbers $m_\pm$; equation (31) still holds, but equations (32)–(33) are replaced with

$$c_\pm=L_{Bick}^2 m_\pm^2 \Omega_1/6R^2=\frac{\overline{\Omega}_1}{3}\left(1\pm\sqrt{1-\frac{3\beta L_{Bick}^2}{2\overline{\Omega}_1\overline{R}}}\right) \tag{34}$$

and

$$2\Omega_1/3-c_\pm=\beta R/m_\pm^2. \tag{35}$$

Solomon *et al.* found that equation (35) was not accurate for westward jets but was within 30% for eastward jets. Our numerical results in Tables III and IV also show that equation (35) is not satisfied by westward jets. However, Tables I and II for the eastward jets also show that for many values of $m_i$ equation (35) has $O(1)$ errors and that the equation's prediction that $2\Omega_1/3-c$ is proportional to $m^{-2}$ is not correct.

Besides being quantitatively incorrect for some parameters of the eastward jets, the Bickley jet model has two major shortcomings. Because it fails qualitatively for the westward jets, it cannot used to explain why the eastward and westward jets differ. Moreover it fails to describe correctly the qualitative features of locking. For low $P$ the Bickley jet is not marginally stable and has two neutral, sinuous modes with independent frequencies $c_\pm$ (i.e., the unlocked flow). With this model,[1] as $P$ increases so does $L_{Bick}$ until $P=P_{lock}$ and the jet is marginally stable. The two waves lock by having $c_+$ slow down continuously to $c_{m.s.}$ and $c_-$ increase continuously to $c_{m.s.}$. This is contrary to observations which show that both speeds decrease abruptly when they lock. Furthermore in the Bickley jet model, the unlocked flow has both Rossby waves centered at the same radial location—the peak of the Bickley jet—which is in contradiction to observations which show two distinct locations of the two waves (fig. 11) with neither at the velocity's peak. Finally, Solomon *et al.* found that for $25<P<65$, the locked eastward jets had $c_i<c_{m.s.}$ and therefore argued that if the locked flows were Bickley jets, they were not marginally stable (and that only the $c_-$ mode was present). However, if the jet is a non-marginally stable Bickley jet, then it poses the question of why the *unstable* eigenmodes with azimuthal wavenumbers with $m_-<m<m_+$ are not present. (Typical values are $m_-=8$ and $m_+=11$ for the parameter range where eastward jets are unlocked.)

## VII. CONCLUSION AND RELEVANCE TO PLANETARY JETS

We have presented a model for the formation of eastward and westward jets on a $\beta$-plane. The underlying assumption is that stirring homogenizes $q$ and that $\beta$ aligns the large-scale velocity into the east–west direction. To test the model we have shown that it quantitatively reproduces laboratory experiments and explains asymmetries between the eastward and westward jets. At low pumping rates $P$, there is one discontinuity in $q$ for each slit. As $P$ increases, $\beta$ causes the westward jets' two discontinuities to move away from each other while the eastward jets' move closer together. Rossby waves travel along the discontinuities, and their speeds $c_i$ differ due to the annular geometry. At $P_{lock}$ the eastward jet's two discontinuities merge causing the two Rossby waves to coalesce and lock with $c_1=c_2$. Because $c_i$ depends on $\Delta q_i$ and because $\Delta q_1$ and $\Delta q_2$ add together when they merge, the $c_i$ decrease when the flow locks. The resulting eastward jet's velocity has a cusp (discontinuity in slope) at its peak, so it is narrow, strong, and wavy (due to the Rossby wave centered at the cusp). Because the westward jet's two discontinuities move apart, they do not, in general, merge together, and the speeds of the two vortex chains rarely lock. The westward jet is weak, has a smooth broad peak, fills most of the annulus, and is not wavy because the Rossby waves are far from the peak and are damped by the tank's boundaries. Both the eastward and westward jets produce chains of vortices in regions where $|\nabla q|$ is small, which for the westward jets is the region between the two discontinuities and for the eastward jets are the two regions that lie between the boundaries of the tank and the nearest Rossby wave. Thus the eastward jets' chains are separated from each other by one (for the locked flow) or two (for the unlocked) discontinuities in $q$, while the westward jets' two chains are in close proximity to (and often

Downloaded 12 Jul 2011 to 169.229.32.136. Redistribution subject to AIP license or copyright; see http://pof.aip.org/about/rights_and_permissions

intertwined with) each other. Because the vortices in the chain are only stable when they have the same sign $\omega$ as the shear of the ambient jet, all of the vortices in the eastward (westward) jet's chain at smaller $r$ have $\omega>0$ ($\omega<0$), while those in the chain at larger $r$ have $\omega<0$ ($\omega>0$). The Rossby wave and its vortex chain travel together at the same speed, but because the flow surrounding the vortices in the chain has nearly uniform $q$, the speeds of the vortices must also approximately match the ambient velocity of the fluid (which is a function of $r$). Thus, the radial locations of the vortices are uniquely determined, and the allowable band of azimuthal wavenumbers of the Rossby wave is constrained. Note that the idealized model flow (which is not smoothed by $\nu$) can differ from the laboratory or numerically-computed flow, but the numbers, locations, speeds and general properties of the waves and vortices agree very well. This is consistent with earlier numerical calculations[18,30] of the waves and vortices of the primary flow (equation (5)) which showed that the waves were sensitive to the values of **U** and $q$ at the flow's discontinuities but insensitive to their values elsewhere. Thus our model, which was designed to simulate the flow at the discontinuities, works very well.

The competing Bickley model for the laboratory experiments fails qualitatively for westward jets and therefore cannot be used to explain the asymmetries between the eastward and westward flows. Moreover, its predicted scalings for eastward flows are incorrect, and it cannot account for wave locking. Our main concern about the Bickley jet model is that it has been used as the starting point of analyses that purport to explain the mixing of tracers in the eastward-jet laboratory flows.[12] Because it is known that large $\nabla q$ or discontinuities in $q$ act as barriers to mixing, because the computed eastward flow and our model of it have strong gradients in $q$, and because the Bickley jet does not, it raises questions about these analyses.

The motivation for our model of the laboratory jets was the fact that we had earlier used the step-function in fig. 2b for the $q$ of the jovian east–west jets. For both the jovian and laboratory flows we initially deduced the jets' $q$ from the properties of the vortices rather than from the direct measurements of the jets' velocities. As fig. 10 shows, the azimuthally-averaged values of $q$ and velocity can be very different from the unaveraged values; averaging disguises a flow's sharp gradients. In both cases our main clue to the functional form of $q$ came from the fact that the vortex chains were located near the maxima of the westward jets and never near the eastward jets.[31] For the laboratory jets we have shown here by direct numerical simulation that our model is accurate, but for Jupiter's jets we still have no direct support of the model in fig. 2. One of the goals of this paper was to support it indirectly by showing that the laboratory experiment, although a crude model of the jovian atmosphere, unambiguously shows that the azimuthal jets in fig. 2 can be created from a flow at rest by forcing it so that its $q$ is stirred and homogenized. Some of the deficiencies of the laboratory flow as a model of Jupiter are that the laboratory experiments produce a step-function $q$ with only one or two steps (whereas the jovian flow has at least 12), the experiments have a highly artificial forcing, and they have an infinite Rossby deformation radius.[5] Although these drawbacks have yet to be overcome in laboratory experiments, they have been in numerical simulations which show that the formation of jets by the homogenization of $q$ is a robust process. In numerical simulations with multiple slits in the bot-

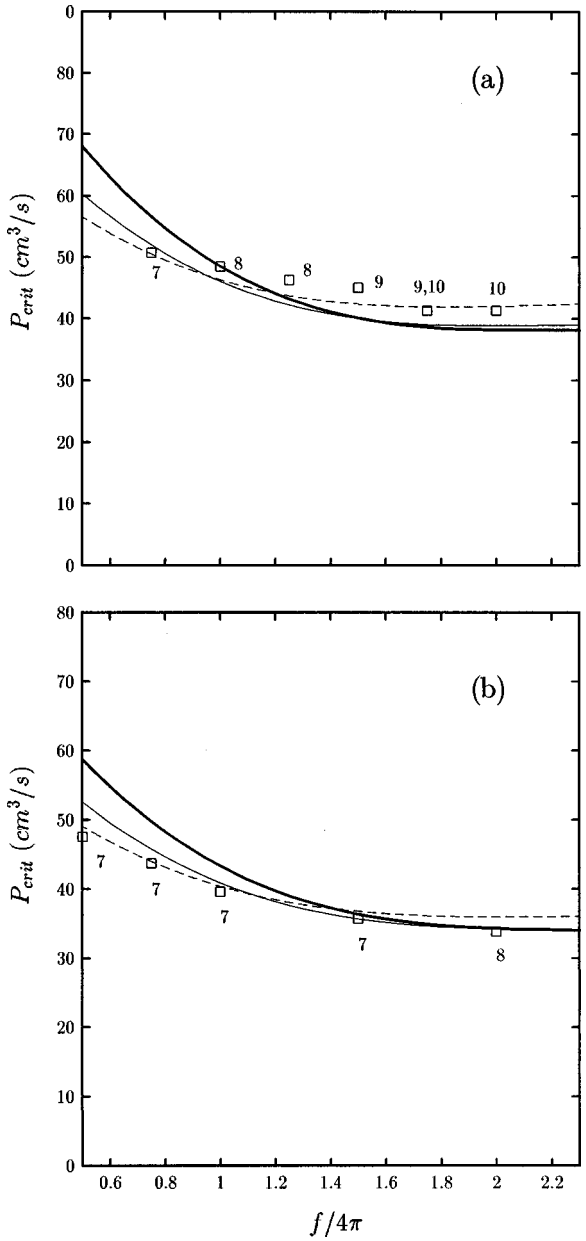


FIG. 13. (a) Numerically computed[15] $P_{crit}$ of the primary eastward jets as a function of $f$ for $\nu=0.1$ and $R_1^{slit}=18.9$ (thick curve for $m=9$, thin for $m=8$, and broken for $m=7$) compared with the laboratory values (shown as squares with the value of $m_{crit}$ written near them). If the numerical calculations and their underlying assumptions are correct, the laboratory value of $P_{crit}$ should correspond to the smallest (as a function of $m$ for fixed $f$) numerically computed value of $P_{crit}$ and the laboratory value of $m_{crit}$ should correspond to the computed curve with the lowest value of $P_{crit}$. (b) Same for the westward jet (thick curve for $m=8$, thin for $m=7$, and broken for $m=6$). The numerical eigenmodes were found by linearizing equations (2) and (3) about the primary $\mathbf{U}(r)$ computed from equation (5) with a parabolic $w(r)$ and $L^{slit}=1.2$. Perturbations are of the form $e^{im(\phi-ct)}$. We used a spectral method with 257 radial collocation points. There were at least 9 points per slit, so the flows were well resolved. Initial-value calculations shows that the instabilities of the primary flow are supercritical.

Downloaded 12 Jul 2011 to 169.229.32.136. Redistribution subject to AIP license or copyright; see http://pof.aip.org/about/rights_and_permissions

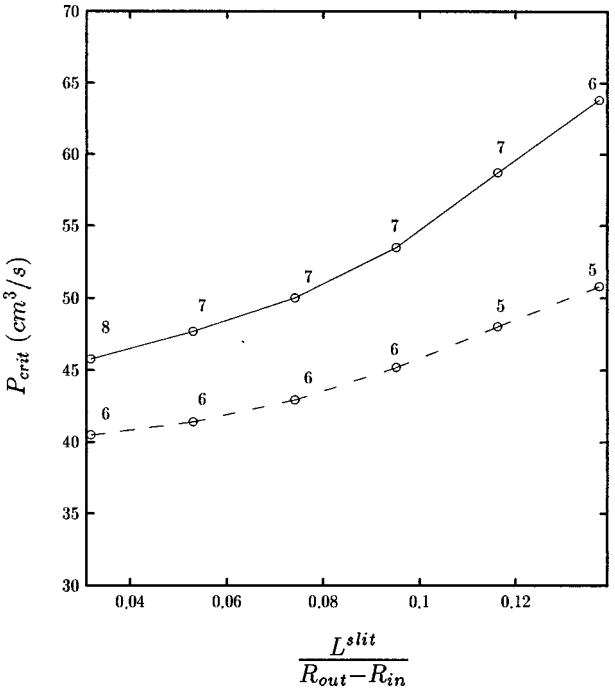


FIG. 14. Numerically computed[15] values of $P_{crit}$ and $m_{crit}$ (shown as integers) of the primary eastward (solid curve) and westward (broken curve) jets as functions of $L^{slit}$ for $\nu=0.1$, $f=4\pi$, and $R_1^{slit}=18.9$. At these values the laboratory eastward jet has $P_{crit}=46.08$ with $m_{crit}=8$, and the westward jet has $P_{crit}=40.41$ with $m_{crit}=7$.

tom boundary, where the pumping direction alternates from slit to slit, the $q$ near each slit is homogenized, and as the pumping increases the homogenized regions grows in size until the discontinuities in $q$ run into each other creating a flow with multiple eastward and westward jets that is well modeled by fig. 2. The model velocity is piecewise parabolic.[32] The eastward jets alternate with the westward jets, with the former strong, narrow, and wavy (due to Rossby waves along the discontinuities) and the latter broad and smooth. Azimuthal flows with step-function $q$ have also been created from a fluid initially at rest in our numerical simulations with a finite Rossby deformation radius,[8] with a more realistic forcing,[8] and with the shallow-water equations.[33] Recent simulations with a realistic forcing (that would correspond to an oscillating grid in a laboratory experiment) show that azimuthal flows with multiple eastward and westward jets (from 4 to 26 of each) can be created where the width of the jets and the spacing between them are unrelated to the scale of the forcing or the boundaries (but is instead set by the strength of the forcing).[34]

Prior to this study, there were few simulations that examined the formation of Jovian-like east–west jets.[35–39] Due to limitations of resolution almost all were two—rather than three-dimensional. Moreover, most were run-down experiments, i.e., with no forcing but with dissipation of the potential enstrophy by a hyper-viscosity. Run-down experiments have severely constrained dynamics due to the fact that they conserve momentum, potential circulation and energy (the latter is due to the reverse cascade and is only approximate). Marcus and Lee[8] showed that if one assumes that a run-down experiment on a $\beta$-plane creates a zonal flow made of axisymmetric bands of uniform $q$ separated by jumps, then the late-time flow has a simple, analytic form that is a function of the initial energy, momentum, circulation (and deformation radius). Thus for run-down experiments to create jovian-like flows, the initial values of these four quantities must be preset to agree with the planetary observations. In contrast, numerical simulations of forced/dissipated flows create zonal winds in which the final flow's energy and strength depend on the balance between forcing and dissipation. We speculate that for the jovian jets to have been stable over hundreds of years of observation, they must also depend on the balance between forcing and dissipation and that the observed flow must be a stable attracting solution for a wide variety of initial conditions and robust with respect to large perturbations. We believe that the formation and maintenance of azimuthal jets by the homogenization of $q$, as illustrated in the experiments and simulations presented here, is an example of how a flow comes to a robust equilibrium, balancing forcing and dissipation, and that this process occurs in a wide variety of laboratory and planetary flows.

## ACKNOWLEDGMENTS

We thank E. Weeks, T. Solomon, H. L. Swinney, and A. Barcilon for helpful discussions. This work was supported by the NSF Planetary Astronomy Program and the NASA Program in Planetary Atmospheres. Computations were carried out at the San Diego Supercomputer Center.

## APPENDIX: APPROXIMATION OF A CIRCULAR ROW OF HOLES WITH AN AXISYMMETRIC SLIT

The pumping in the laboratory experiment is through two concentric rows of 120 holes in the bottom boundary of the annulus. In equation (3) the rows of holes are approximated as circular slits of effective width $L^{slit}$. We have argued the reasonableness of this approximation and found the value of $L^{slit}$ that corresponds to the experiment:[30] $L^{slit} \simeq \sqrt{H}(P/8\pi N)^{1/4}(f\nu)^{-1/8}$ where $N$ is the number of holes in a row. For typical parameter values, this is $\sim 1.5$ times the Stewartson layer thickness $\sqrt{\tau\nu}$ and much larger than a hole diameter. The value of $L^{slit}$ is determined by viscous diffusion (which increases it to Stewartson layer thickness) and also by the circumferential velocity about each hole. One test of the slit approximation, as well as the quasi-geostrophic approximation, is fig. 13 which compares the laboratory measurements of $P_{crit}$ and $m_{crit}$ (the $m$ of the unstable eigenmode) to the values computed from the linearized form of equations (2) and (3)). The agreement is good. However, we caution the reader that the agreement depends upon the value of $L^{slit}$ (fig. 14).[40]

[1] J. Sommeria, S. D. Meyers, and H. L. Swinney, ''Experiments on vortices and Rossby waves in eastward and westward jets,'' in *Nonlinear Topics in Ocean Physics*, edited by A. Osborne (North-Holland, Amsterdam, 1991), p. 227.
[2] J. Sommeria, S. D. Meyers, and H. L. Swinney, ''Laboratory model of a planetary eastward jet,'' Nature (London) **337**, 58 (1989).
[3] T. H. Solomon, W. J. Holloway, and H. L. Swinney, ''Shear flow instabilities and Rossby waves in barotropic flow in a rotating annulus,'' Phys. Fluids A **5**, 1971 (1993).
[4] J. Sommeria, S. D. Meyers, and H. L. Swinney, ''Laboratory simulation of

Downloaded 12 Jul 2011 to 169.229.32.136. Redistribution subject to AIP license or copyright; see http://pof.aip.org/about/rights_and_permissions

Jupiter's Great Red Spot,'' Nature (London) (London) **331**, 689 (1989).
[5]J. Pedlosky, *Geophysical Fluid Dynamics*, 2nd ed. (Springer, Berlin, 1986).
[6]P. S. Marcus, ''Jupiter's Great Red Spot and other vortices,'' Annu. Rev. Astron. Astrophys. **431**, 523 (1993).
[7]In the atmospheric literature eastward jets, which flow from west to east, are ''westerlies.''
[8]P. S. Marcus and C. Lee, ''Jupiter's Great Red Spot and zonal winds as a self-consistent, one-layer, quasigeostrophic flow,'' Chaos **4**, 269 (1994).
[9]S. S. Limaye, ''Jupiter: New estimates of the mean zonal flow at the cloud level,'' Icarus **65**, 335 (1986).
[10]B. A. Smith, L. Soderblom, R. Batson, P. Bridges, J. Inge, H. Masursky, E. Shoemaker, R. Beebe, J. Boyce, G. Briggs, A. Bunker, S. A. Collins, C. J. Hansen, T. V. Johnson, J. L. Mitchell, R. J. Terrile, A. F. Cook, II, J. Cuzzi, J. B. Pollack, G. E. Danielson, A. P. Ingersoll, M. E. Davies, G. E. Hunt, D. Morrison, T. Owen, C. Sagan, J. Veverka, R. Storm, and V. E. Suomi, ''A new look at the Saturnian system: The Voyager 2 Images,'' Science **215**, 504 (1982).
[11]D. A. Godfrey, ''A hexagonal feature around Saturn's North Pole,'' Icarus **76**, 335 (1988).
[12]D. del-Castillo-Negrete and P. J. Morrison, ''Chaotic transport by Rossby waves in shear flow,'' Phys. Fluids A **5**, 948 (1993).
[13]P. B. Rhines and W. R. Young, ''Homogenization of potential vorticity in planetary gyres,'' J. Fluid Mech. **122**, 347 (1982).
[14]Numerical calculations are spectral with Fourier modes in the azimuthal and Chebyshev modes in the radial direction. The method has no splitting errors due to the fractional steps. Details are in Refs. 18 and 20.
[15]For all laboratory experiments and numerical calculations $s=-0.1$, $H=18.7$, $R_{in}=10.8$, $R_{out}=43.2$, $R_2^{slit}=35.1$, and $16<P\leqslant 100$ in CGS units. The values of $\nu$, $f$, and $R_1^{slit}$ vary. In the annular geometry $\beta<0$ while in the Cartesian (which replaces $r$ with $(-y)$) $\beta>0$. For pumping rates near $P_{lock}$, the Reynolds number of the vortex chains (defined as the circulation of a vortex divided by $\nu$) is $\sim 500$, the Rossby number (based on their vorticities divided by $f$) is $\sim 0.1$ and the Ekman spin-down time $\tau \simeq T$ where $T$ is the characteristic turn-around time of a vortex.
[16]P. S. Marcus, ''Numerical simulations of Jupiter's Great Red Spot,'' Nature (London) **331**, 693 (1988).
[17]Another, but less general, way to show how pumping creates **F** is to note that pumping creates a weak, ageostrophic, radial velocity that starts at one slit and ends at the other: $v_{ag}\simeq \pm P/2\pi rH$ for $R_1^{slit}<r<R_2^{slit}$ and is zero elsewhere. Note that $\nabla\cdot v_{ag}\hat{\mathbf{r}}\neq 0$ and the $v_{ag}$ is not part of the QG **U** in equation (2) ($\nabla\cdot\mathbf{U}\equiv 0$, so there is a stream function: $\mathbf{U}=\hat{\mathbf{z}}\times\nabla\psi$). The rotation of the annulus acts upon the ageostrophic velocity to create a Coriolis acceleration $v_{ag}\hat{\mathbf{r}}\times f\hat{\mathbf{z}}$ which is equivalent to **F** in equation (3). One could include the Coriolis acceleration due to **U**, $\mathbf{U}\times f\hat{\mathbf{z}}$, in equation (2), but it is equal to $\nabla(f\psi)$, so it can be incorporated into the definition of $\Pi/\rho$ (when $\rho$ is constant) and is not included.
[18]C. Lee, ''Basic instability and transition to chaos in a rapidly rotating annulus on a $\beta$-plane ,'' Ph. D. dissertation, University of California at Berkeley, 1993.
[19]P. S. Marcus, ''Spatial self-organization of vortices in chaotic shearing flows,'' Nucl. Phys. B, Proc. Suppl. **2**, 127 (1988).
[20]P. S. Marcus, ''Vortex dynamics in a shearing zonal flow,'' J. Fluid Mech. **215**, 393 (1990).
[21]L. M. Polvani, J. Wisdom, E. DeLong, and A. P. Ingersoll, ''Simple dynamical models of Neptune's Great Dark Spot,'' Nature (London) **249**, 1393 (1990).
[22]L. M. Polvani and J. Touma, ''A note on recent experiments with Rossby waves on eastward jets'' in *Nonlinear Phenomena in Atmospheric and Ocean Sciences*, edited by G. Carnevale and R. Pierrehumbert (1991).
[23]P. G. Drazin and W. H. Reid, *Hydrodynamic Stability* (Cambridge University Press, Cambridge, 1981).
[24]For the westward jet model (in an unbounded domain) $\chi$ is given by: $\chi(1+k_0)-2=[\chi(1-k_0)+2]\,\eta e^{-2k(a+b)}$ where $\eta\equiv[k-k_1\pm(k_1+k)e^{-2(Y_2^{slit}-a)k_1}]/[k+k_1\pm(k-k_1)e^{-2(Y_2^{slit}-a)k_1}]$ where $k_1\equiv k\sqrt{1+2/\{k(a+b)[k(a+b)-\chi]\}}$ and $k_0=\sqrt{1-2/[k\chi(a+b)]}$. The upper (lower) sign in the definition of $\eta$ is for eigenmodes that are symmetric (anti-symmetric) about $y=0$. For eastward jets, the eigenmodes are always symmetric; otherwise, there is no disturbance of the contours of constant $q$ at $y=0$ which is contrary to the laboratory and the numerically calculated flows, but for westward jets the eigenmodes could be antisymmetric, although in the initial-value calculations and experiments they are always symmetric. For $Y_2^{slit}=a$, $\eta$ is $+1$ for symmetric and $-1$ for antisymmetric modes. Tables III and IV are computed with symmetric modes. For eastward jets with (with one or two discontinuities) $\chi$ approximately satisfies $\chi(k_0+1)-2=[\chi(k_0-1)+2]e^{-kk_0(|Y_1^{slit}-Y_2^{slit}|-2a)}$ with fractional errors of $O(e^{-2k(a+b)}/k^2(a+b)^2)$. If there are boundaries within a distance $L_b$ of the discontinuities, then there are additional fractional errors in both expressions for $\chi$ of order $e^{-2kL_b}$. Under most circumstances the wavenumbers of interest are large and the discontinuities are far from the boundaries, so $k(a+b)$ and $kL_b$ are large, the fractional errors are small, and the boundary locations do not usually affect $c$. For eastward jets, the fractional errors in $[\overline{u}(y_d)-\overline{c}]$ in equation (27) contain the errors inherent in $\chi$ from above as well as errors of $O(e^{-2kk_0(Y_2^{slit}-a)})$. For the westward jets, equation (27) has fractional errors of $O(e^{-2k(a+b)}/k^2(a+b)^2, e^{-2kL_b})$ for $2k(Y_2^{slit}-a)\gg 1$ and $O(e^{-2k(a+b)}, e^{-2kL_b})$ otherwise.
[25]The dispersion relation for a flow as in fig. 8b has been previously published. L. D. Talley, ''Radiating barotropic instability,'' J. Phys. Oceanogr. **13**, 972 (1983).
[26]Our model flows also have Rossby waves that are not localized to the locations where there are jumps in $\overline{q}$. These eigenmodes are sines and cosines in $y$ rather than exponentials. They exist in regions where $\overline{u}$ is constant and are similar to the usual Rossby waves in a channel with $\overline{c}\simeq\overline{u}-\beta/[k^2+(n\pi D)^2]$ where $n$ is an integer and $D$ is the width of the region of constant $\overline{u}$. Since there is no forcing in the regions of constant $\overline{u}$, there would be no reason for these modes to be excited. Indeed, our numerical calculations show no evidence of these channel Rossby waves, so we do not consider them.
[27]$\Delta q_2$ and $c_2$ are further reduced by the proximity of $R_{out}$ to $R_2^{slit}$. Note that $\Delta q_2$ is equal to $\beta(a_2+b_2)$. The value of $b_2$ in the numerical calculation is smaller than that predicted by the model because the model's value of $(R_2^{slit}+b_2)$ is greater than $R_{out}$ which is impossible.
[28]E. Weeks and T. Solomon (private communication, 1995).
[29]The location of the outer discontinuity in $q$ is much closer to $R_{out}$ than a Rossby wavelength, typically 5% of a wave length or less than 2 cm.
[30]C. Lee and P. S. Marcus, ''Eastward and westward jets in a rotating annulus model of a barotropic atmosphere,'' in the *Proceedings of the CERCA Workshop in Semi-analytic Methods in Turbulence*, edited by K. Coughlin (Montreal, Canada, 1997).
[31]The large uncertainties in the averaged jovian velocities make it necessary to infer $q$. We carried out run-down experiments where the initial flow consists of an axisymmetric, east–west velocity superposed with noise. We varied the initial velocity and examined the speeds, shapes, and locations of the vortices that formed.[6] The best results were with the initial $q$ of the east–west velocity approximately equal to a step-function. Use of the traditional sinusoidal east–west velocity was particularly bad. When the initial $q$ was approximately a step function, the chains of cyclonic and anti-cyclonic vortices were intertwined and centered at the westward jets, similar to the observed jovian vortex streets. An initially sinusoidal east–west velocity produced vortex chains widely spaced in latitude with each chain located near a local zero of the east–west velocity. Inclusion of a finite Rossby deformation radius in the QG equations or use of the shallow-water equations made these results even more pronounced.
[32]The authors have also used a model with finite Rossby deformation radius to examine these jets.[8] In this case $\overline{u}$ is a series of connected $cosh$ functions rather than parabolas.
[33]S. Kim, ''Dynamics of the Great Red Spot and Jovian Zonal Flows,'' Ph. D. thesis, University of California at Berkeley, 1996).
[34]P. S. Marcus and C. Lee, ''Two-dimensional turbulence and the formation of $\beta$-jets with forcing and dissipation'' (in preparation).
[35]R. L. Panetta, ''Zonal jets in wide baroclincally unstable regions–Persistence and scale selection,'' J. Atmos. Sci. **50**, 2073 (1993).
[36]S. A. Condie and P. B. Rhines, ''A convective model for the zonal jets in the atmospheres of Jupiter and Saturn,'' Nature (London) **367**, 711 (1994).
[37]G. Williams, ''Jovian and comparative atmospheric modeling,'' Adv. Geophys. **28A**, 381 (1985).
[38]J. Y.-K. Cho and L. M. Polvani, ''The morphogenesis of bands and zonal winds in the atmospheres on the giant outer planets,'' Science **273**, 335 (1996).
[39]J. Y.-K. Cho and L. M. Polvani, ''The emergence of jets and vortices in

Downloaded 12 Jul 2011 to 169.229.32.136. Redistribution subject to AIP license or copyright; see http://pof.aip.org/about/rights_and_permissions

freely evolving, shallow-water turbulence on a sphere,'' Phys. Fluids **8**, 1531 (1996).

[40]Computations with parabolic, Gaussian, and top-hat $w(r)$ with the same $L^{slit}$ give the same $P_{crit}$ to within 1%, where $L^{slit}$ is the full width at half maximum of $w(r)$. Figures 13 and 14 used a parabolic $w(r)$. In principle, one could use the experimental values of $P_{crit}$ with fig. 14 to determine the best value of $L^{slit}$ to use in numerical computations. However, this method cannot be used at $P>P_{crit}$ because the ''best'' value of $L^{slit}$ depends on $P$: $L^{slit}$ controls the vortex layer's thickness. As $L^{slit}$ increases, the $\omega(r)$ at each slit goes from a delta function to a function with width approximately equal to $L^{slit}$. With $\nu\to 0$ equation (5) shows that $u$ of the primary flow is approximately independent of $L^{slit}$, so at each layer

$$q \simeq \frac{\mp f\tau P}{2\pi H R_i^{slit} L^{slit}} + \beta R_i^{slit}.$$

As the layers roll-up into discrete vortices, the $q$ of each vortex is approximately conserved at its initial value. Thus, $L^{slit}$ determines the strength of the vortices in the chains. With $\nu\to 0$ equation (5) also shows that the potential circulation of the layers and chains are nearly independent of $L^{slit}$; therefore, the areas of the vortices must depend on $L^{slit}$.

Downloaded 12 Jul 2011 to 169.229.32.136. Redistribution subject to AIP license or copyright; see http://pof.aip.org/about/rights_and_permissions